

Comparison of winding-number sequences for symmetric and asymmetric oscillatory systems

Volker Englisch

17712 Crystal Spring Terrace, Ashton, Maryland 20861, USA

Ulrich Parlitz*

Biomedical Physics Group, Max Planck Institute for Dynamics and Self-Organization, Am Faßberg 17, 37077 Göttingen, Germany
and Institute for Nonlinear Dynamics, Georg-August-Universität Göttingen, Am Faßberg 17, 37077 Göttingen, Germany

Werner Lauterborn

Drittes Physikalisches Institut, Georg-August-Universität Göttingen, Friedrich-Hund-Platz 1, D-37077 Göttingen, Germany

(Received 4 June 2014; revised manuscript received 22 December 2014; published 14 August 2015)

The bifurcation sets of symmetric and asymmetric periodically driven oscillators are investigated and classified by means of winding numbers. It is shown that periodic windows within chaotic regions are forming winding-number sequences on different levels. These sequences can be described by a simple formula that makes it possible to predict winding numbers at bifurcation points. Symmetric and asymmetric systems follow similar rules for the development of winding numbers within different sequences and these sequences can be combined into a single general rule. The role of the two distinct period-doubling cascades is investigated in the light of the winding-number sequences discovered. Examples are taken from the double-well Duffing oscillator, a special two-parameter Duffing oscillator, and a bubble oscillator.

DOI: [10.1103/PhysRevE.92.022907](https://doi.org/10.1103/PhysRevE.92.022907)

PACS number(s): 05.45.Ac, 05.45.Pq

I. INTRODUCTION

Nonlinear dynamical systems generically reveal a complexity in their response to periodic excitation beyond any expectation. Even the simplest nonlinear extension of the harmonic oscillator, the single-well Duffing oscillator $\ddot{x} + d\dot{x} + x + x^3 = 0$, a passive system with just one fixed point, shows a response behavior to periodic driving only marginally explored because of its incredible complexity; see, for instance, the early studies on the subject [1–4], as well as the more recent ones [5,6] that are, however, for large driving only. Despite continued efforts (see, for example, the topological approach by Gilmore and Lefranc [7]), the state of knowledge still leaves much space for further investigations inasmuch as nonlinear systems and periodic driving are ubiquitous in nature, as daily, monthly, and annual periods show.

Among those systems to be investigated first on the way to improving our understanding, nonlinear oscillators form an important class, displaying coherent behavior. Different oscillators as the just mentioned simple Duffing oscillator, a bubble in a liquid set into oscillation by a sound field [8,9] and a pump-modulated laser oscillator [10] exhibit topologically similar bifurcation sets in parameter space [11]. A recurrent structure made up of repeated, complex units that can be traced back to the resonances of the system is consistently found for the bifurcation set. This means that a single resonance and its inner structure can be considered as a building block for other resonances of the system. This inner structure has only partially been explored because it shows an infinity of bifurcation sequences that could not yet be delineated.

In this article, the role of winding numbers for describing the bifurcation set of nonlinear oscillators is further explored, in particular, the fine structure inside a single resonance, as

an extension of previous work on the sinusoidally driven double-well Duffing oscillator [12]. This Duffing system can be described in normalized form (i.e., with dimensionless quantities) by the three-parameter equation,

$$\ddot{x} + d\dot{x} - x + x^3 = f \cos(\omega t), \quad (1)$$

where d is the damping parameter, and f and ω represent the amplitude and the angular frequency of an external driving force, respectively. Because of the “−” sign in front of x and the “+” sign in front of x^3 , this system is called the (−,+)-Duffing oscillator. Correspondingly, the first mentioned type of Duffing oscillator is called the (+,+)-Duffing oscillator and the type investigated by Bonatto *et al.* [5] and Stefanescu [6], where the linear term in the restoring force is missing, gets the name (0,+)-Duffing oscillator. The (0,+)-Duffing oscillator can be regarded as the limiting form of the (+,+)- and (−,+)-Duffing oscillators in the case of large driving [13,14].

The (−,+)-Duffing oscillator also shows a recurrent structure in the bifurcation set. This structure is, however, more involved than in the (+,+)-Duffing system mentioned above, because the free system $\ddot{x} + d\dot{x} - x + x^3 = 0$ has three fixed points. Two of them are stable; one is unstable. The repeating structures, i.e., building blocks, are first noticed in the more accessible bifurcation diagrams, where one variable of the system (x or $v = \dot{x}$) is plotted against a parameter of the system in a Poincaré section plane (mostly ω here). Figure 1 presents one such diagram of Eq. (1) for the fixed parameters $f = 10$ and $d = 0.2$. Up to 16 different initial conditions have been taken for each frequency not to miss (the most prominent) coexisting attractors. Four of the higher harmonic resonances are shown and labeled $R_{10,1}$, $R_{12,1}$, $R_{14,1}$, and $R_{16,1}$. The second index of these labels is the period number that indicates the period of the response in relation to the driving period. Thus, “1” means the same period as the driving. The first index denotes the torsion number l , which has been

*ulrich.parlitz@ds.mpg.de

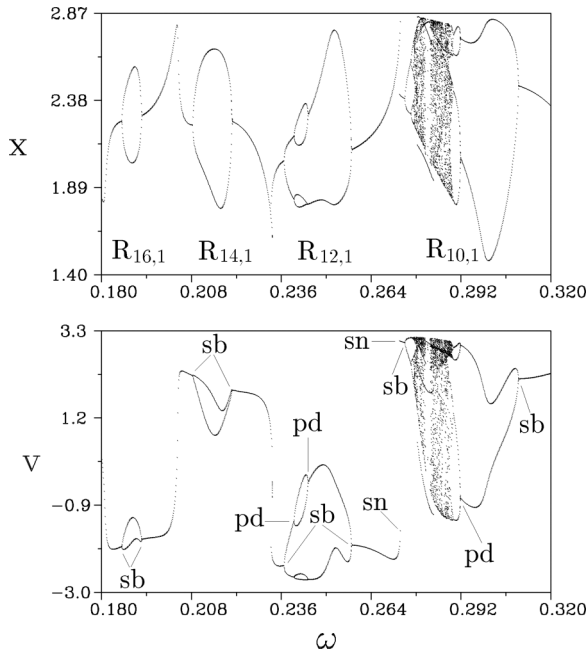


FIG. 1. Bifurcation diagrams of the $(-,+)$ -Duffing oscillator for $f = 10$ and $d = 0.2$ that show the recurrent structure of resonances and their bifurcational evolution for x and $v = \dot{x}$. Four resonances with their four pairs of symmetry-breaking (sb) bifurcations are covered. Additionally, the resonances labeled $R_{12,1}$ and $R_{10,1}$ show period-doubling (pd) bifurcations. In the resonance $R_{10,1}$ a complete period-doubling cascade to chaos including a period-3 window and two saddle-node (sn) bifurcations show up (see [12] for further details).

found useful in classifying the individual nonlinear resonances (building blocks of the bifurcation set). The torsion number gives the number of torsions, in units of 2π , of an orbit that is infinitesimally near to a periodic one around that orbit; see [15–17]. Four cross sections through resonances with increasing complexity are present within this figure with four pairs of symmetry-breaking (sb) bifurcations, an additional pair of period-doubling (pd) bifurcations in the resonance $R_{12,1}$ and a complex bifurcation structure in the resonance $R_{10,1}$ including chaotic bands with periodic windows, and a pair of saddle-node (sn) bifurcations. These four cross sections also give an impression of the evolution of a single resonance when the driving force f is increased or the damping d is decreased, starting from Fig. 1.

When a single bifurcation, for instance a period-doubling bifurcation, is followed in the three-dimensional parameter space $\{(d, f, \omega)\}$, it forms a distinct structure often called “resonance horn” because of its characteristic shape. As an example, the horn associated with the period-2 bifurcation in the main resonance $R_{1,1}$ of the $(-,+)$ -Duffing system [Eq. (1)] is shown in Fig. 2.

The horn represents a period-doubling bifurcation surface that occurs for small driving amplitudes only, when the motion of a particle is restricted to one side of the potential well and its behavior can be described by that of an asymmetric system. The interior of such a resonance horn may be filled with chaotic regions which themselves are interrupted by a

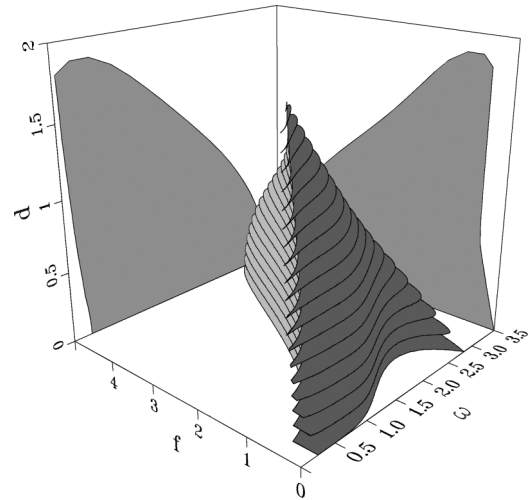


FIG. 2. The bifurcation surface of the first period-doubling bifurcation in the main resonance ($R_{1,1}$) in the three-dimensional parameter space of the $(-,+)$ -Duffing oscillator [Eq. (1)]. Outside of this bifurcation horn a stable period-one orbit exists, whereas the period-one orbit is unstable within the horn. Immediately below the surface of the horn, in its interior, a period-doubled oscillation exists. For increasing values of the damping coefficient d the horn is getting smaller in cross section and vanishes above a critical value of $d^* \approx 1.871$.

large number of periodic windows. Specific regularities in the occurrence of the periodic windows exist for the $(-,+)$ -Duffing system [12]. These regularities suggest (among others, e.g., period-doubling cascades) an increase of the period of periodic windows up to infinity, called period adding [18,19], when increasing (or decreasing) some bifurcation parameter. This goes along with a distinct regularity of winding numbers for sn bifurcations forming winding-number sequences.

Figure 3 shows the ω -bifurcation diagram for the x coordinate in a Poincaré section plane of the resonance $R_{6,1}$ for $f = 1$ and $d = 0.2$: the full resonance is essentially covered in the top diagram, while the bottom diagram shows the phenomenon of period adding from period 3 onwards for decreasing ω towards the limit ω_{\min} for the resonance $R_{6,1}$ denoted by ω_{\min}^6 , where the oscillation returns to a simple oscillation with the period of the excitation.

Throughout this paper, this sequence will serve as one example for the winding-number sequence investigation including the first level of subwindows. Furthermore, its connection with period-doubling cascades is investigated. Fixed-point diagrams and phase diagrams in parameter space are used to complete the view. Additional examples are drawn from the Duffing oscillator $\ddot{x} + c\omega\dot{x} + x^3 = \cos(\omega t)$, called $(c\omega)$ -Duffing oscillator, due to its two-dimensional parameter space $\{(c, \omega)\}$ and easier handling of resonances. The bubble oscillator (see [9]) is used as a typical example of an asymmetric oscillator. It has recently found strong interest (see, for instance, [9,20–23]) both experimentally and theoretically because of the unique single bubble measurement technique in an acoustic bubble trap found by Gaitan *et al.* [24]. From the results of symmetric and asymmetric oscillators a general rule is derived for winding-number sequences inside resonances.

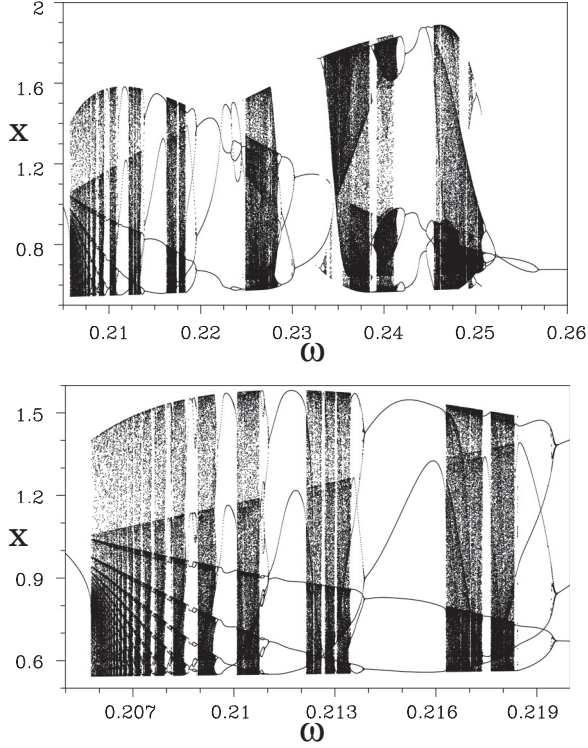


FIG. 3. Bifurcation diagrams (x coordinate in a Poincaré section plane versus ω) for the resonance $R_{6,1}$ with $f = 1$ and $d = 0.2$. (Top) Essentially full view of the resonance. (Bottom) Magnification of the lower-frequency part of the top diagram to highlight the period-adding phenomenon. The period-adding sequence runs to the left and starts with a window of period 3.

II. WINDING-NUMBER SEQUENCES OF SYMMETRIC SYSTEMS

Englisch and Lauterborn [12] have shown that certain periodic windows can be grouped together when investigating the fixed-point loops of the most prominent windows to compose winding-number sequences. For the windows with low periods, it has been found that the ω -parameter intervals, where a period- $(q + 1)$ orbit exists, are always subsets of the interval of the q window. Here, q is the *symmetry period number* defined as

$$q = \begin{cases} m_0 & \text{if the orbit is symmetric,} \\ 2m_0 & \text{if the orbit is asymmetric,} \end{cases} \quad (2)$$

where m_0 is the basic period number (oscillation period $T = m_0 2\pi/\omega$) and symmetric (or asymmetric) refers to the shape of the orbit in the $x-\dot{x}$ plane. This definition implies that q is odd for symmetric orbits and even for asymmetric orbits. The fixed-point loops are frequency interlocked and it holds $[\omega_{q+1, \min}, \omega_{q+1, \max}] \subset [\omega_{q, \min}, \omega_{q, \max}] \forall q \in \mathbb{N}_0$.

The *symmetry torsion number* p is defined similarly to the symmetry period number q ,

$$p = \begin{cases} n_0 & \text{if the orbit is symmetric} & (q \text{ odd}), \\ 2n_0 & \text{if the orbit is asymmetric} & (q \text{ even}), \end{cases} \quad (3)$$

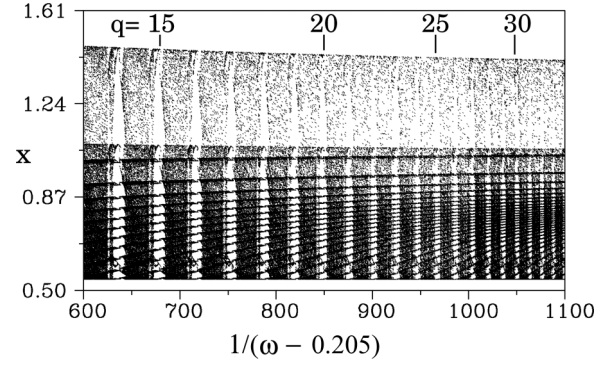


FIG. 4. Bifurcation diagram for the $(-,+)$ -Duffing oscillator from inside the resonance $R_{6,1}$ ($f = 1, d = 0.2$) for the x coordinate in a Poincaré section plane versus $1/(\omega - 0.205)$ instead of ω to emphasize the period-adding window structure. Some windows are labeled by their symmetry period number q .

where n_0 is the ordinary torsion number [15–17]. These definitions have been introduced to assist in the formulation of laws for the bifurcation sequences inside resonance horns.

The *winding number* is then defined as

$$w = \frac{p}{q}. \quad (4)$$

The winding numbers $w_k^l = p_k^l/q_k^l$ for the sn bifurcations with symmetry period number q_k^l and symmetry torsion number p_k^l ($k = 1, 2, 3, \dots$; $l =$ torsion number of the resonance) have been found to obey the law [12]

$$w_k^l = \frac{p_k^l}{q_k^l} = \frac{(l-1) + (l+1)(k-1)}{k}, \quad k = 1, 2, 3, \dots \quad (5)$$

To arrive at Eq. (5), the relative width of a window has been used as the deciding factor for building bifurcation sequences. The width has been compared with neighboring windows in order to make a decision as to whether that window belongs to the given sequence of “main” windows. The selection can be made intuitively convincing when looking at Fig. 4. For clarity of representation, we choose to plot data as a function of $1/(\omega - 0.205)$. The convergence point ω_{\min}^6 is located near $\omega = 0.205$, which therefore moves to near infinity in Fig. 4 when the quantity $1/(\omega - 0.205)$ is plotted along the abscissa. In this diagram it can clearly be seen that the widths of the periodic windows are comparable in size and therefore are the natural choice to form a sequence. The sizes of the windows are still visibly shrinking for very high periodic windows, i.e., periods $q > 30$. This can be explained with the point of convergence that is obviously off by a small amount from the chosen value of $\omega = 0.205$.

A. Subwindows within the main chaotic bands

As mentioned above and seen in Fig. 4, a chaotic band exists between each two main windows with their symmetry period numbers q and $q + 1$. These bands contain a large number of periodic windows within, whose ordering is investigated in this paragraph. The following bifurcation diagrams of the $(-,+)$ -Duffing system [Eq. (1)], given in Fig. 5, are magnifications of the first three main chaotic bands from the

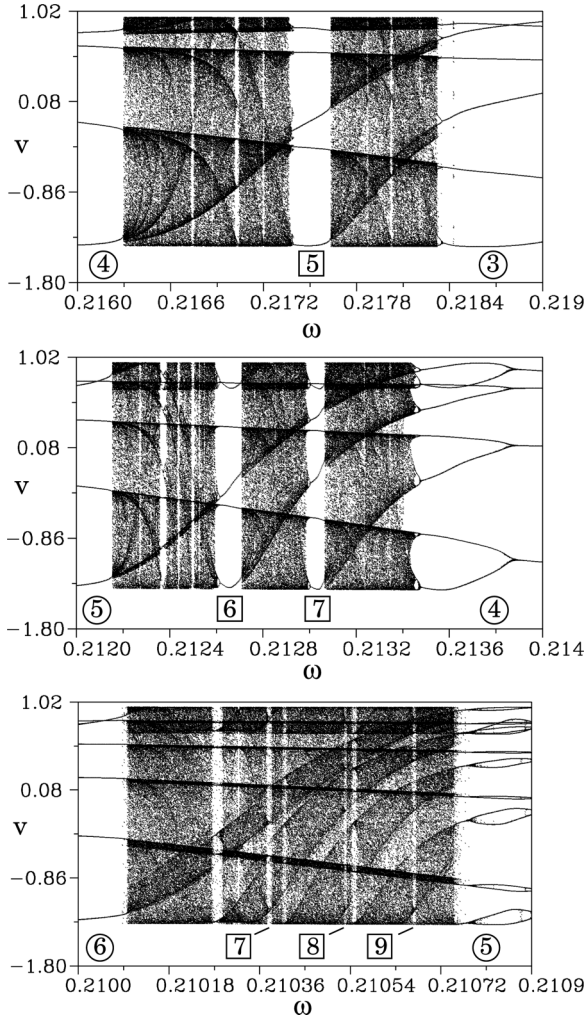


FIG. 5. Bifurcation diagram for the $(-,+)$ -Duffing oscillator from inside the resonance $R_{6,1}$ ($f = 1, d = 0.2$) for the v coordinate in a Poincaré section plane versus ω with subwindows between the main windows of symmetry period number $q = 3$ and 4 (top), $q = 4$ and 5 (middle), and $q = 5$ and 6 (bottom).

period-adding sequence whose higher-order periods are given in Fig. 4. They are bound by the main windows with the symmetry period numbers $q = 3$ and 4 , $q = 4$ and 5 , and $q = 5$ and 6 , respectively.

In Fig. 5, top diagram, several periodic windows are seen within the first chaotic band which exists between the main windows $q = 3$ and $q = 4$. The bounding symmetry period numbers q are shown encircled in this and the following figures. Note that the first pd bifurcation for the $q = 3$ window lies outside the depicted area at larger ω (compare Fig. 3). One periodic window dominates and is roughly located in the middle of the chaotic region: It is marked by its symmetry period number $q_s = 5$ and is framed by a square to visually distinguish it from all others. Whereas the circle around the symmetry period numbers denotes the main windows, the square represents a first generation of subwindows. The symmetry period numbers of these subwindows are distinguished from the other windows of the main period-adding sequence by the subscript “s”. The subwindow $q_s = 5$ in

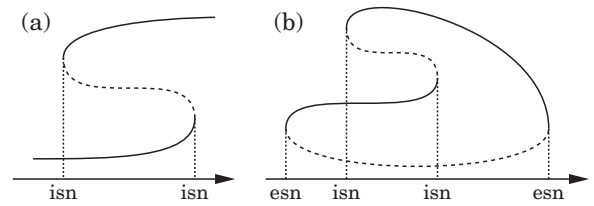


FIG. 6. Pictograms of an interior saddle-node (isn) bifurcation pair and an exterior saddle-node (esn) bifurcation pair. (a) Hysteresis region of a nonlinear oscillator resonance with two stable branches (solid lines) between the two saddle-node bifurcations denoted by isn and one unstable branch (dashed line) that connects the two stable branches. Outside the two isn bifurcations only one stable solution of the same period exists. (b) An isn-bifurcation pair can only occur after generation of an orbit of period $m_0 > 1$ by an esn bifurcation. Outside the parameter values of the esn bifurcation no solution with period m_0 exists. (Only one branch of the m_0 coexistent fixed-point branches is shown.)

Fig. 5, top diagram, comes into existence by a sn bifurcation of a symmetric period-5 solution and arises by an exterior saddle-node bifurcation [25] that generates a period-5 attractor.

A distinction is made between the *interior* saddle-node (isn) bifurcations and the *exterior* saddle-node (esn) bifurcations [25]. Saddle-node bifurcation points that belong to resonance curves that turn over and give rise to the phenomenon of hysteresis are called isn bifurcations. This type of bifurcation leads to coexisting attractors of the same period and evolves from an existing period [Fig. 6(a)]. Conversely, for an esn bifurcation only one stable and one unstable orbit exist that are connected at the bifurcation point ω [Fig. 6(b)]. The orbit is born without the prior existence of another orbit of the same period. Locally, there are no differences between an exterior and an interior saddle-node bifurcation. It is therefore necessary to include additional global information to identify whether a given sn bifurcation is of the type esn or isn. Throughout this work, fixed-point diagrams have been calculated to obtain this additional global information. These fixed-point diagrams show a specific loop structure, as well as sequences of stable and unstable sections of the fixed-point curve. This additional information assists in selecting the windows and helps to classify isn and esn bifurcations. Exterior saddle-node bifurcations give rise to a closed loop structure in fixed-point diagrams; interior ones can only be connected via exterior ones in order to close a loop (Fig. 6).

There are other periodic windows inside the chaotic bands to the left and to the right of the subwindow $q_s = 5$ in Fig. 5, top diagram. These are not considered for this particular investigation because either their size is much smaller compared to the one of the period-5 subwindow or these windows are not formed by an esn bifurcation. This procedure—the selection of periodic windows by determining their relationship with each other and some of their specific properties—has already been used to successfully identify the main windows and therefore has been applied to identify these subwindows as well.

Within the second chaotic band shown in Fig. 5, middle diagram, there are two dominant windows marked with their symmetry period number $q_s = 6$ and $q_s = 7$. Again these

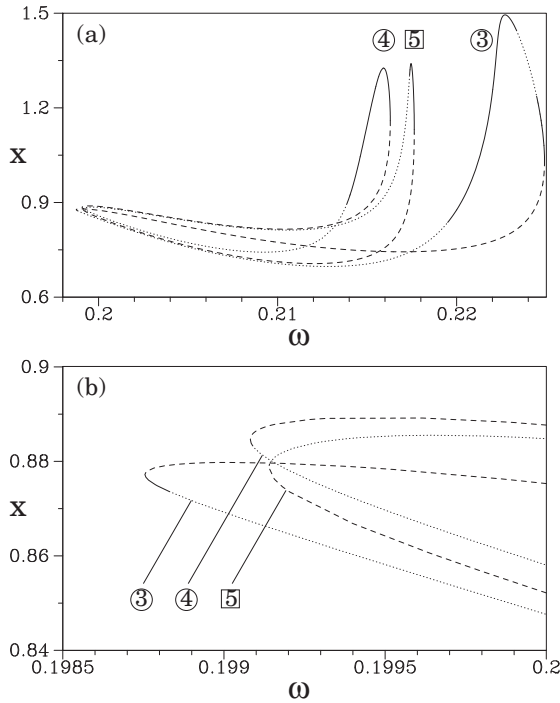


FIG. 7. (a) Fixed-point curves of the two main and the one dominant subwindows that correspond to the subwindows with the same numbers in the bifurcation diagram given in Fig. 5, top diagram. (b) Enlargement of the low-frequency end to show the interleaving sequence connected with the different windows. Solid line, stable solutions; dashed line, unstable solution by a sn bifurcation; dotted line, unstable solution by a pd bifurcation.

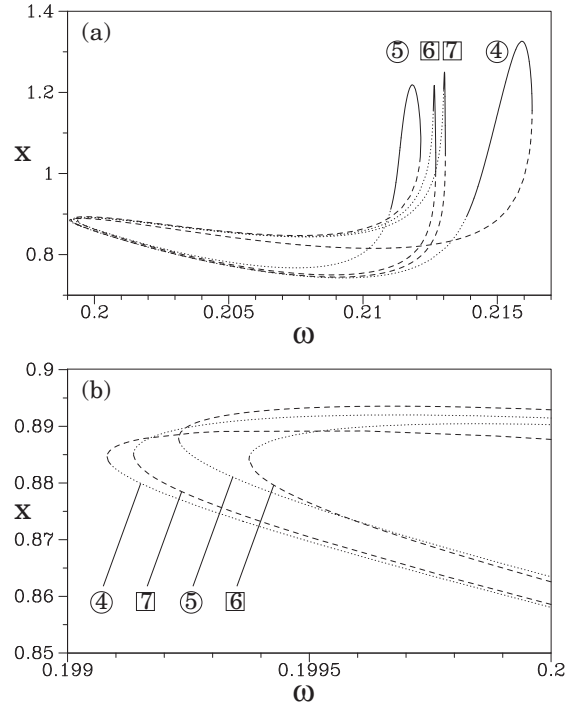


FIG. 8. (a) Fixed-point curves of the two main windows and the two subwindows corresponding to the two subwindows with the same numbers in the middle bifurcation diagram of Fig. 5. (b) Enlargement of the low-frequency end to better show the interleaving sequence connected with the different windows. Note how the parameter range of the periodic windows that exist on the ω -frequency axis is always confined by the frequency range of its successor within its sequence. Line style as in Fig. 7.

windows originate from an esn bifurcation. The window $q_s = 6$ consists of two coexisting asymmetric attractors of period $m_0 = 3$, the window $q_s = 7$ consists of one symmetric attractor of period $m_0 = 7$.

The next chaotic band of this series exists between the two main windows with symmetry period numbers $q = 5$ and $q = 6$ (Fig. 5, bottom diagram). Within this chaotic region there are six periodic subwindows of recognizable size. Only three of these windows—those labeled with their symmetry period number $q_s = 7, 8, 9$ —fulfill the criteria to be generated by an esn bifurcation. These are considered for further investigation. The other three windows are found to arise by regular isn bifurcations. Looking at the symmetry period numbers q_s of these three chaotic bands shown, a period-adding sequence for the q_s within each of the following chaotic bands can be expected.

As already discussed in [12], the fixed-point curves of the subwindows within a chaotic band show different patterns compared to those found for the main windows (which are frequency interlocked). Fixed-point curves for the main windows and the subwindows of first order are given in Figs. 7 to 9. These figures correspond to the bifurcation diagrams in Fig. 5. For better visualization, just one of the q or q_s coexisting fixed-point loops are shown in these figures. These loops have been picked such that all the loops for the different symmetry period numbers are shown for corresponding fixed points of their cycle.

For the subwindows it may be seen that the parameter range of their existence on the ω -frequency axis is not restricted by the frequency range of the main windows. Although the high frequency end of the subwindows lies in between two of the main windows, this does not completely hold for the low-frequency ends. However, it is true for the subwindows among one another and it holds that $[\omega_{q_s-1, \min}, \omega_{q_s-1, \max}] \subset [\omega_{q_s, \min}, \omega_{q_s, \max}] \forall q_s \in \mathbb{N}$, which can be seen from Figs. 8 and 9. This characteristic has been found for all investigated sets of subwindows and is similar to the frequency-interlocking phenomena of the main windows. However, there is the difference in that the periodic subwindows of *higher* symmetry period number q_s are confining the sequences of *lower* symmetry period number. In other words, a fixed-point loop of symmetry period number q can only be found where a fixed-point loop of symmetry period number $q - 1$ already exists. In contrast, a subwindow $q_s - 1$ can only be found where a fixed-point loop of symmetry period number q_s already exists. These subwindows themselves can only be found where a main window of symmetry period number $q > (q_s/2)$ already exists.

Figure 9(c) shows an enlargement of the high-frequency range of Fig. 9(a). Comparing Fig. 9 with the bottom bifurcation diagram in Fig. 5, it becomes apparent why three of the six windows seen inside the chaotic band were neglected. The neglected windows do not directly fit into the series of

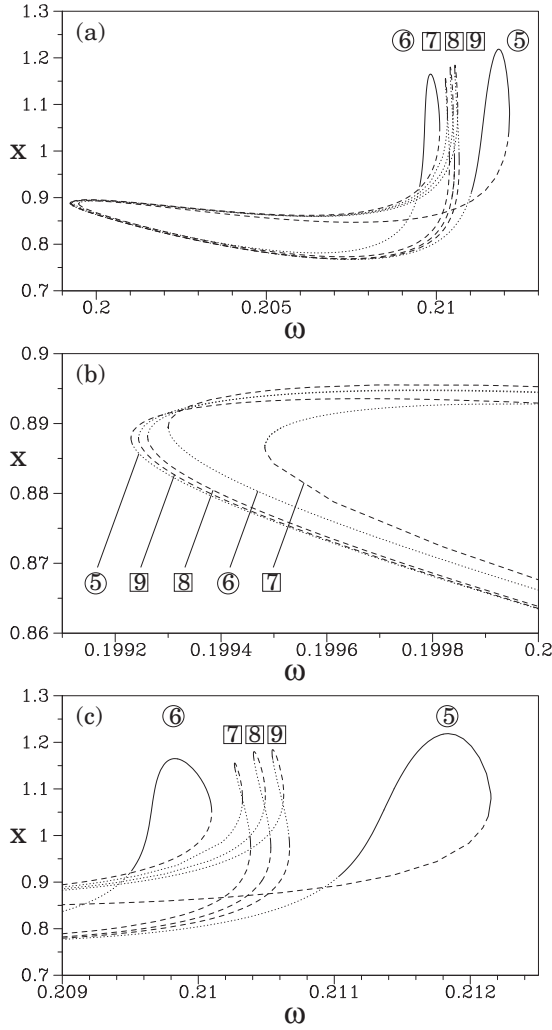


FIG. 9. (a) Fixed-point curves of the two main and the three subwindows that correspond to the subwindows with the same numbers in the bifurcation diagram given in Fig. 5, bottom diagram. (b) Enlargement of the low-frequency end to better show the interleaving sequence connected with the different windows. Again, the ω -frequency limits of one fixed-point curve is roughly determined by those of its successor. (c) Enlargement of the upper frequency part of the fixed-point diagram. It can easily be noticed that three of the six periodic windows shown in the bottom diagram of Fig. 5 are created by an isn bifurcation. Line style as in Fig. 7.

periodic windows because the windows are formed due to a hysteresis of the fixed-point loops (i.e., the tips of the loops) and are therefore isn bifurcations. This example shows why fixed-point curves are essential for these investigations: Only with the information provided by the fixed-point loops is it possible to objectively classify subwindows originating by an isn or esn bifurcation.

For clarification of the organization of the periodic windows, these are now arranged in a schematic diagram (Fig. 10). Each window is shown and represented by its symmetry period number q for the main windows or q_s for the subwindows, respectively. As already shown in Fig. 5, the symmetry period numbers of the main windows are encircled, whereas the symmetry period numbers of the subwindows are each framed

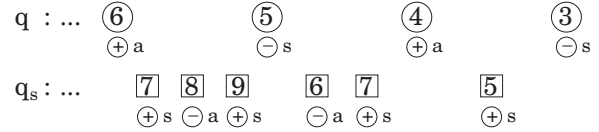


FIG. 10. Symbolic arrangement of the windows and subwindows. The letters “a” and “s” denote asymmetric and symmetric oscillations, respectively. The symbols \oplus and \ominus indicate the type of winding-number sequence according to the two types of pd-bifurcation sequences [15–17]. They are discussed in the next section, where the connection of winding number and period doubling is investigated.

by a square. The “a” in this scheme indicates a sn bifurcation of two asymmetric orbits. The “s” stands for the occurrence of a single symmetric orbit. The \oplus and \ominus signs are discussed in the next section in connection with the two different types of period-doubling cascades.

From this diagram we can infer the following.

(1) The number of subwindows of the first level, N_s , within the parameter range bordered by two sn bifurcations of the main window sequence with symmetry period number q and $q + 1$ is given as

$$N_s^q = q - 2, \tag{6}$$

which implies that the number of subwindows within consecutive chaotic bands increases by one:

$$N_s^{q+1} = (q + 1) - 2 = (q - 2) + 1 = N_s^q + 1. \tag{7}$$

(2) The symmetry period numbers of the N_s^q subwindows are given as

$$q_s = q + 2, \dots, 2q - 1, \tag{8}$$

where the windows with the higher symmetry period number are ordered in such a way that they appear at higher driving frequencies when looking at the maximum of the fixed-point loops (or vice versa at the minimum end).

In the same way that the periods m of the subwindows are governed by the ones of the main windows, this is also true for the winding numbers of the corresponding esn bifurcations. The winding numbers for the $q = 5$ and $q = 6$ main windows are given as $w_5^6 = 33/5$ and $w_6^6 = 40/6$. The corresponding chaotic region contains the subwindows with the winding numbers at the esn bifurcations as $w(q_s = 7) = 47/7$, $w(q_s = 8) = 54/8$, and $w(q_s = 9) = 61/9$. This shows that the winding numbers of the subwindows are the same as the winding numbers of the main windows with the same symmetry period number. It also proves to be true for the other subwindow sequences investigated and it is reasonable to derive the winding numbers $w_{q,j}^l$ of the subwindows from those of the main windows w_q^l in the following way:

$$w_{q,j}^l = w_{(q+1)+j}^l, \quad j = 0, \dots, q - 2 = N_s^q. \tag{9}$$

Here the notation $w_{q,j}^l$ is describing the winding number of the j th subwindow of the resonance $R_{l,1}$, which follows the main window with symmetry period number q . According to Eq. (6), exactly $q - 2$ subwindows exist within each chaotic band. However, the index j in Eq. (9) starts at $j = 0$, therefore leading to one more window. This additional window has been included in the sequence to characterize the fact that

the “subwindow” for $j = 0$ is equivalent to the main window $q + 1$. The winding-number sequence can thus be considered as starting from that value.

B. Winding-number sequences and period-doubling cascades

Up to this point the winding numbers of esn bifurcations have been investigated. In this paragraph, the winding numbers along pd cascades that lead to chaotic bands are considered instead.

It is known from various studies [15–17] that the development of the winding numbers along a pd cascade is governed by the torsion of the local flow in units of 2π for the closed orbit and that the winding number of the k th pd bifurcation can be written as

$$\bar{w}_k = \bar{w}_\infty \pm \frac{(-1)^k}{3m_0 2^k}, \quad k = 0, 1, 2, 3, \dots, \quad (10)$$

with m_0 being the basic period of the orbit, i.e., the period from where a pd cascade starts. The value of the limiting winding number \bar{w}_∞ is given by

$$\bar{w}_\infty = \bar{w}_0 \mp \frac{1}{3m_0}. \quad (11)$$

As these two equations indicate, there are two kinds of pd sequences: one with the winding number decreasing at the transition from \bar{w}_0 to \bar{w}_1 —according to the + sign in Eq. (10)—and one with the winding number increasing from \bar{w}_0 to \bar{w}_1 according to the – sign. In Fig. 10, these two types of cascades are marked as \oplus - and \ominus -type cascades according to the sign in Eq. (10).

When comparing the cascades of the main windows with those for the subwindows, it may be seen that both types show slightly different behavior. For the main windows a pd cascade of the \ominus type can be found for every window with an odd symmetry period number ($q = m_0$) and thus the orbit is symmetrically born. On the other hand, the \oplus type can be found for all even symmetry period numbers. The behavior of the pd cascades of the subwindows has been found to behave the other way around.

We now concentrate on the winding numbers along the pd cascade of the sequence of main windows and subwindows to compare these two types. We use the resonance $R_{6,1}$ again as an example like we did in our previous investigations. In Fig. 11, the winding numbers along the periodic windows are written horizontally and the occurring pd cascades of these windows are listed in a vertical manner (also compare the first two rows of the figure with Fig. 10).

The top row of Fig. 11 indicates the type of the pd cascade that can be found within that particular window, e.g., a \oplus - or \ominus -cascade according to Eq. (10). Although a fully developed pd cascade could not be found for every periodic window before the chaotic band sets in, it should be possible to always find such a cascade for a suitable path through the parameter space.

As an example of how this diagram should be interpreted, the second column that represents the pd cascade of the main window with the symmetry period number $q = 6$ is explained in detail below as it is followed downwards. This main window comes into being by a sn bifurcation—marked in the third

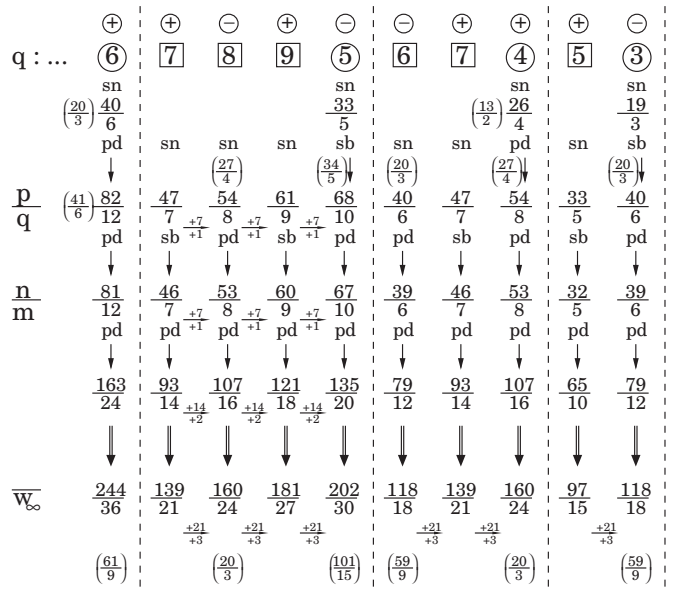


FIG. 11. Scheme that shows the arrangement for the main and subwindows of the resonance $R_{6,1}$ and their pd sequences. Horizontally, the sequence of the windows are given; vertically, the winding numbers of the pd sequences belonging to them are given. For more details, see the text.

row—with the symmetry period number of $w_0^6 = 40/6$ at that bifurcation. Since two asymmetric orbits occur simultaneously (q is even), the winding number w , written as a fraction of the torsion number n and the period m_0 , is given as $w_0^6 = 20/3$. This value is shown in parentheses with an even torsion number. Therefore, the following pd cascade of a main window must be one of the \oplus type (\ominus if it were a subwindow). The first bifurcation of an asymmetric orbit within the cascade must then be a pd bifurcation (marked as pd in the fifth row) with a winding number $\bar{w}_1 = 41/6$ at the bifurcation. For the winding numbers along a pd cascade, the notation \bar{w} is used instead of w . The notation \bar{w} describes the winding number defined by Eq. (10), whereas w describes the winding number just for the sn bifurcations along a window sequence described by Eq. (5). As can be seen from the diagram of Fig. 11, both sequences are intertwined because the winding number at the window sequence represents the first element of winding numbers along a pd cascade: $w_6 = \bar{w}_0$.

Another pd bifurcation follows $\bar{w}_1 = 41/6$, which leads to the winding number $\bar{w}_2 = 81/12$ and so on. The winding numbers of the pd cascade converge towards the limiting value $\bar{w}_\infty = 244/36$ [Eq. (11), third last row indicated by \bar{w}_∞] [15,17,26]. The resulting fraction for \bar{w}_∞ is an expanded fraction to show the relation to the corresponding values of neighboring periodic windows. Where it applies, the reduced fraction is written in the last row of the diagram.

Each row of this diagram can be read in the same way. The type of the bifurcation occurring in each case is listed between each two rows of winding numbers. Below the row, marked as n/m , only pd bifurcations occur. Above it, the type of bifurcation depends on whether the orbit is born as a symmetric or an asymmetric solution and whether the pd cascade occurs within a main window or a subwindow.

It should be noticed that it is possible to group blocks of pd cascades which are marked by vertical dashed lines. Within these blocks small subsequences of winding numbers exist. These subsequences have already been identified in Fig. 10. Each block, i.e., subsequence, is built by the N_s^q existing subwindows along with one of the two confining main windows, i.e., the one with the smaller symmetry period number q .

The winding numbers $w_{q,j}^l$ of the subwindows of the rows marked as p/q correspond to the ones described by Eq. (9). A possible explanation for the number N_s^q of subwindows given by Eq. (6) can now be guessed. Looking at the left block and starting with the subwindow that has a symmetry period number $q_s = 7$ (second column, row p/q , in Fig. 11) and proceeding to the right towards the main window $q = 5$, the symmetry torsion number p_s increases for every subwindow by $\Delta p = 7$ as already has been found for the main windows. Similarly the symmetry period number increases by $\Delta q_s = 1$. Assuming a hypothetical fourth subwindow within this chaotic band following the window with $q_s = 9$, the corresponding winding number had to be $w_{q,j}^l = w_{5,4}^6 = 68/10$. This, however, is the winding number of the first bifurcation (a sb bifurcation) of the main window $q = 5$ (written as $w = p/q$). Therefore, it is possible to include the main window and its pd cascade into this subsequence. The same behavior can be found for all the other blocks of subsequences and, naturally, it can be found on every level of pd bifurcations, bearing in mind that Δp and Δq have to be multiplied by two for every additional level of pd bifurcations viewed.

It is now possible to write down the winding number of the subwindows at the sn bifurcation from Eq. (9) in a modified form:

$$\begin{aligned} p_{q,0}^l &= p_q^l, & q_{q,0}^l &= q_q^l, & l &= 0, 2, 4, 6, \dots, \\ w_{q,j}^l &= \frac{p_{q,j}^l}{q_{q,j}^l} = \frac{p_{q+1}^l + j(l+1)}{q_{q+1}^l + j} \\ &= \frac{(l-1) + (l+1)(q+j)}{q+j+1}, & j &= 1, 2, \dots, q-2. \end{aligned} \quad (12)$$

The equation describes the winding number of the j th subwindow within a chaotic band that is following the q th main window of the resonance l .

Also, the limiting values \bar{w}_∞ for all the cascades can be calculated, when the value of one cascade is known, or from the torsion number n_0 and its period m_0 . For the former, it yields that the value \bar{w}_∞ increases its symmetry torsion number by $\Delta p = 3(l+1)$ for neighboring subwindows while the symmetry period number increases by $\Delta q = 3$:

$$\begin{aligned} \bar{w}_\infty(q_{s+1}) &= \frac{\bar{p}_\infty(q_s) + 3(l+1)}{\bar{q}_\infty(q_s) + 3} \\ &= \frac{3[n_0(q_s) + (l+1)] \mp 1}{3[m_0(q_s) + 1]}, \end{aligned} \quad (13)$$

with $\bar{p}_\infty(q_s)$, $\bar{q}_\infty(q_s)$ denoting the numerator and denominator of the fraction $\bar{w}_\infty(q_s)$.

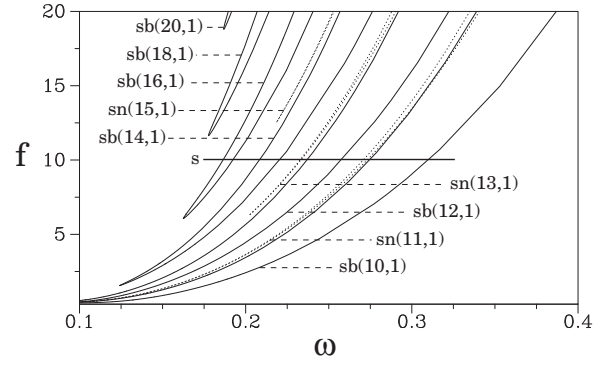


FIG. 12. Phase diagram for the resonance horns $R_{10,1}$ to $R_{20,1}$ of the $(-,+)$ -Duffing oscillator for $d = 0.2$. The horizontal line with the label “s” indicates the parameter range for which the bifurcation diagram has been given in Fig. 1.

III. WINDING-NUMBER SEQUENCES IN THE PARAMETER SPACE

Until now, only one-dimensional cross sections of the three-dimensional parameter space have been investigated by means of bifurcation diagrams and fixed-point curves. In this section it is shown that the findings of the previous chapters are not due to a particular path through the parameter space but will also hold on a more general level. For this purpose, two-dimensional phase diagrams are investigated.

A phase diagram is a condensed or two-dimensional bifurcation diagram [2,3,11]. As an example for a simple phase diagram, we consider Fig. 12. The figure shows the global structure of the resonances $R_{n,1}$, $n = 10, 11, \dots, 20$, for the $(-,+)$ -Duffing oscillator [Eq. (1)] in parameter space. Each resonance shown, from $R_{10,1}$ to $R_{20,1}$, is marked by its type of bifurcation (sn or sb), as well as the torsion number n and the period number m (first and second numbers in parentheses). The bifurcation lines belonging to the resonances $R_{17,1}$ and $R_{19,1}$ do not reach all the way down into the plot range chosen and are therefore not visible. The thick line at $f = 10$ parallel to the ω axis and marked by the letter “s” represents a cross section for which the bifurcation diagram has been given in Fig. 1.

As an example, one of the sb resonances—choosing again the resonance $R_{6,1}$ —is shown in more detail. In Fig. 13 the inner structure of the sb resonance is shown, also reflecting the behavior of the winding-number sequences in the parameter space.

The sb bifurcation $sb(6,1)$ is shown with a dotted line style. Within the line of the sb bifurcation the bifurcation curves of the esn bifurcations for the windows $q = 3, 4, \dots, 8$ are noted. The right borders of these resonances are marked with their respective torsion number and period number. The left parts of the bifurcation lines are lying so close to each other that they appear to be just one single thick line. It has already been emphasized that the fixed-point curves of windows with high symmetry period number are bordered by those of smaller periodic windows. Since none of the corresponding bifurcation curves are crossing each other (within the investigated area), we surmise that this behavior also holds within a large range in the parameter space. However, it should be noted that for

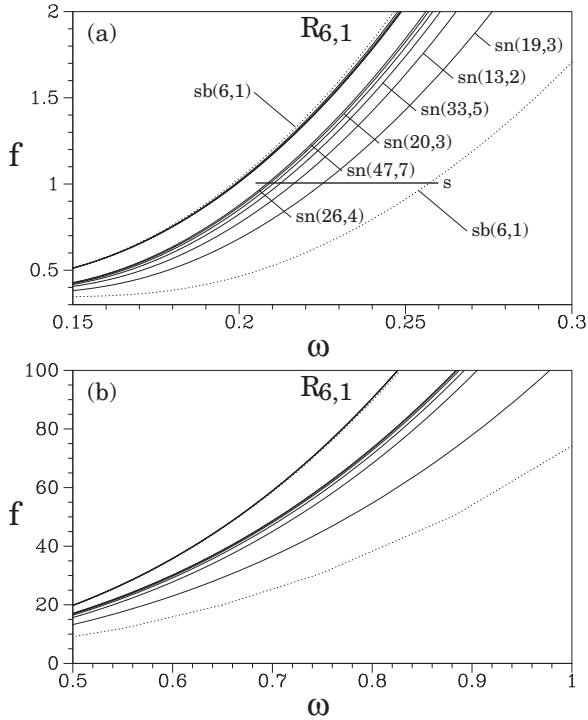


FIG. 13. (a) Phase diagram for the resonance horn $R_{6,1}$ of the $(-,+)$ -Duffing oscillator for $d = 0.2$. The horizontal line with the label “s” indicates the parameter range for which the bifurcation diagram has been given in Fig. 3. The resonances are marked with their respective period and torsion number. (b) The same as (a) with the parameter range greatly extended.

much higher driving amplitudes, $f \gtrsim 40$ [Fig. 13(b)], the line of the $sb(6,1)$ bifurcation is crossing the sn -bifurcation lines of the periodic windows.

From Figs. 12 and 13 it can be seen that the resonances of the $(-,+)$ -Duffing oscillator are represented by very narrow, stretched objects. Because the resonance curves become very narrow and stretched at low frequency, which makes their numerical and graphical resolution hard, we consider a modified Duffing system. This modified Duffing system shows approximately the same behavior as that of Eq. (1) but its resonances in parameter space appear to be more conveniently arranged. The system has been called the $(c\omega)$ -Duffing oscillator [27] and reads

$$\ddot{x} + c\omega\dot{x} + x^3 = \cos(\omega t). \quad (14)$$

This system can be derived from Eq. (1) in the limit of large amplitudes and by introducing a constant damping d per driving period such as $d = c\omega$. The transformation also leads to a two-parameter system with the parameters now being the angular driving frequency ω and the dissipation parameter c . To compare the phase diagrams of both systems, the resonance $R_{6,1}$ of the $(c\omega)$ -Duffing system is presented in Fig. 14.

The bifurcation curve for the sb bifurcation is plotted as a dotted line; the sn -bifurcation curves for the periodic windows are shown as solid lines. For the four sn bifurcations in this figure their corresponding torsion and period numbers are used to label the curves. It may be seen that the winding numbers for these bifurcation curves are the same as the

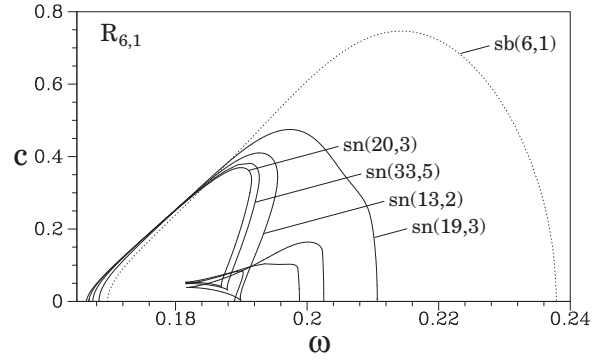


FIG. 14. Phase diagram for the resonance horn $R_{6,1}$ of the $(c\omega)$ -Duffing system that gives the sn -bifurcation curves of the first periodic windows with period number $m = 3, 2, 5, 3$ corresponding to the symmetry period number $q = 3, 4, 5, 6$.

winding numbers of the resonance $R_{6,1}$ of the $(-,+)$ -Duffing system. These bifurcation curves—in contrast to the ones of the $(-,+)$ -Duffing oscillator—have a global maximum, which can be explained by the transformation of the parameters [28].

However, despite its advantages with respect to the presentation, some disadvantages occur when using this transformation of the Duffing system. In particular, the bifurcation curves for the higher periodic sn bifurcations of the $(c\omega)$ -Duffing are not located completely inside one another, i.e., the ones with a lower period. This phenomenon is getting more obvious the smaller the value of the dissipation parameter c is chosen. Two possible reasons could lead to this result. The first one is due to the choice of parametrization. For two different points in the parameter space with a constant value of dissipation c , the damping d of the original system [Eq. (1)] differs. This difference could lead to the observed “deformation” of the bifurcation structure compared to the one of the $(-,+)$ -Duffing system. The second reason could be of principle interest. As shown in Fig. 13, the bifurcation curve $sb(6,1)$ of the symmetry-breaking bifurcation is crossing the bifurcation curves of the periodic windows for high driving amplitude f . The sb curve is crossing the sn curves at lower c values for higher resonances. Since a low dissipation constant for the $(c\omega)$ -Duffing system corresponds to a high driving amplitude of the $(-,+)$ -Duffing system, it could be expected that for very high amplitudes f of the $(-,+)$ -Duffing system the bifurcation curves of the sn bifurcations will also cross each other, or, for very high resonances ($\omega \rightarrow 0$) for which the systems approach the same behavior, only the sb curve will cross the sn curve. This will need further investigation elsewhere.

The interpretation of bifurcation curves of the $(c\omega)$ -Duffing oscillator should be done carefully, however. It is not always obvious whether a bifurcation curve can be evaluated as an inner or exterior bifurcation curve. Although for the bifurcation points of a fixed-point curve the definition is straightforward for what could be called an esn or an isn , a bifurcation curve with a self-crossing region can belong to an esn as well as an isn bifurcation. Therefore, other criteria must be called upon with the different types of sn bifurcations.

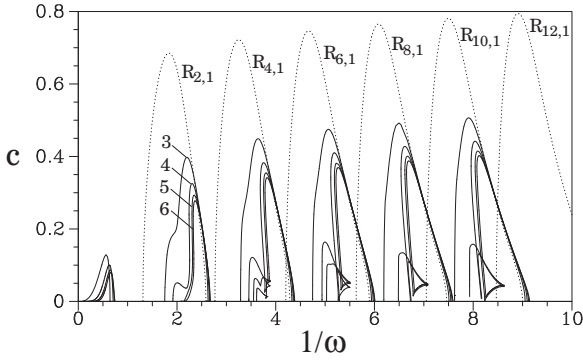


FIG. 15. Phase diagram for the first few harmonic resonances of the $(c\omega)$ -Duffing system. Given are the sb-bifurcation lines (dotted) and the sn-bifurcation lines (solid) for $q = 3, 4, 5, 6$ inside each resonance (marked in $R_{2,1}$).

IV. EXTENSION OF WINDING-NUMBER SEQUENCES

In the previous section, as well as in [4,11,25,29–31] (see also the experiments by Klinker *et al.* [32]), it has been shown that a resonance can be divided approximately into two halves with an isn bifurcation that separates these two parts [for a resonance $R_{2n,1}$, these two parts would be separated by a $sn(2n,1)$ curve]. In Fig. 15, all of the sb resonances $R_{2,1}$ to $R_{12,1}$ are shown, including sn bifurcations building the winding-number sequences $w_k^l, l = 0, 2, 4, \dots, 10$. The x axis in this diagram is chosen as $1/\omega$, because the resulting harmonic resonances occur in almost equidistant steps. Again, the sb curves are shown as dotted lines in order to distinguish them from the sn-bifurcation curves. In this figure, the winding-number sequence for each resonance resides within one “half” (on the right hand side) of that resonance. This might suggest that there is still “space” in between every two winding-number sequences for another sequence within the left “half” of every sb resonance. We thus question whether it might be possible to find a second window sequence with bifurcation curves that are located between the ones already found. This is investigated for the rest of this section.

When the sn-bifurcation curves of Fig. 15 are arranged according to periods and size of the denominator, the following sequence of winding numbers representing all period-3 curves occurs:

$$\begin{aligned} \frac{1}{3} \rightarrow \frac{2}{3} \rightarrow \frac{7}{3} \rightarrow \frac{8}{3} \rightarrow \frac{13}{3} \rightarrow \frac{14}{3} \rightarrow \frac{19}{3} \rightarrow \frac{20}{3} \rightarrow \\ \rightarrow \frac{25}{3} \rightarrow \frac{26}{3} \rightarrow \frac{31}{3} \rightarrow \frac{32}{3} \rightarrow \dots \end{aligned} \quad (15)$$

The integer part for all these fractions (when written as a decimal number) is even and the winding number is always a reduced fraction. The fractions with even torsion numbers represent the bifurcations, for which asymmetric trajectories come into existence and symbolize the windows whose symmetry period number is $q = 6$. The fractions with odd torsion numbers represent the bifurcations, where a single symmetric orbit is born and whose symmetry period number is $q = 3$. Because bifurcations for which the nominator of a winding number $w = n/m$ is a multiple of the denominator (e.g., $0/3, 3/3, 6/3, \dots$) were never found in our investigations,

it is assumed hereafter that such bifurcations cannot exist (also see Discussion). Again, when using this type of presentation for the bifurcation curves it is assumed that there is still “space available” between each two existing winding numbers of period-3 orbits for another set of winding numbers possibly building a second winding-number sequence within each resonance. These “missing” winding numbers would include the fractions $4/3, 5/3, 10/3, 11/3, \dots$

Whether the assumption that esn-bifurcation curves with integer winding numbers exist as expanded fractions remains an open question. It is not known yet if their existence can entirely be ruled out or if they are only difficult to find numerically because their basins of attraction in phase space are too tiny. Assuming this type of winding number does exist, it must also be possible to find an esn bifurcation of period 1.

In correspondence to Eq. (15) a winding-number sequence for the bifurcation curves built by the period-2 orbits can be written as

$$\frac{1}{2} \rightarrow \frac{5}{2} \rightarrow \frac{9}{2} \rightarrow \frac{13}{2} \rightarrow \frac{17}{2} \rightarrow \frac{21}{2} \rightarrow \dots \quad (16)$$

and similarly for the bifurcation curves of period 5:

$$\frac{3}{5} \rightarrow \frac{13}{5} \rightarrow \frac{23}{5} \rightarrow \frac{33}{5} \rightarrow \frac{43}{5} \rightarrow \frac{53}{5} \rightarrow \dots \quad (17)$$

None of the winding-number sequences that have been found up to now contain a symmetric orbit of period 2. Therefore, all the fractions in Eq. (16) represent bifurcation curves that belong to windows with symmetry period number $q = 4$. Again, assuming bifurcations with integer winding numbers do not exist (e.g., $0/2, 2/2, 4/2, \dots$), this would leave “space” for one winding number between every two elements of the sequence noted in Eq. (16) (e.g., $3/2, 7/2, 11/2, \dots$). Similar arguments can be found for Eq. (17) when keeping in mind that only the winding number for the symmetry period number $q = 5$ (symmetric orbit) has been calculated and the ones for $q = 10$ (asymmetric orbit) are missing here, e.g., $4/5, 14/5, 24/5 \dots$

From the reasoning above, there are strong indications that for every resonance $R_{2n,1}$ a second, not yet observed winding-number sequence should be able to be calculated. The winding numbers of this second “missing” sequences should be such that the sequences Eqs. (15)–(17) of the two winding-number sequences combined contain every possible fraction of the given period (denominator).

Indeed, these bifurcation curves have also been found numerically and their winding numbers can be arranged in the same regular manner as their counterpart. For every resonance $R_{2,1}, \dots, R_{12,1}$, a second sequence of periodic windows exists. The bifurcation curves for the symmetry period number $q = 3, \dots, 7$ are all shown in Fig. 16, which is being given with the same parameter area as has been used for Fig. 15. All the winding numbers of these bifurcation curves were missing within the respective sequences of Eqs. (15)–(17). The corresponding bifurcation lines are shown in Figs. 17 and 18, respectively.

In the same way as found earlier—for the first type of winding-number sequences—the odd symmetry period number indicates the existence of one single symmetric orbit

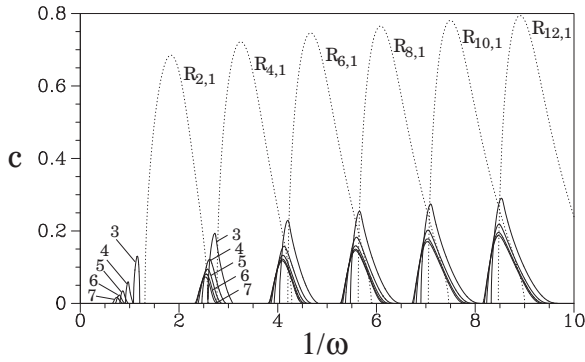


FIG. 16. Phase diagram for the first few resonances of the $(c\omega)$ -Duffing system. Given are the sb-bifurcation lines (dotted) and the second winding-number sequence of sn-bifurcation lines (solid) for $q = 3, 4, 5, 6, 7$ inside each resonance (marked for the main resonance and in $R_{2,1}$).

and the even symmetry period number points to two coexisting orbits.

When forming a winding-number sequence out of these bifurcations just found—in the same manner as has been done

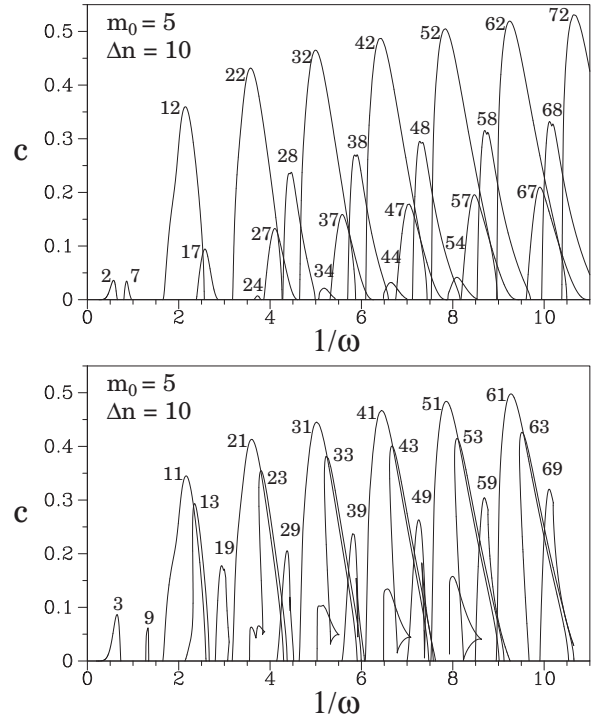


FIG. 18. The first few bifurcation lines generated by an esn bifurcation of period 5 for the $(c\omega)$ -Duffing oscillator. Seven of the presumably eight existing classes are given, distributed on two diagrams for better readability. The individual eight (displayed seven) classes all have torsion numbers with the same last digit.

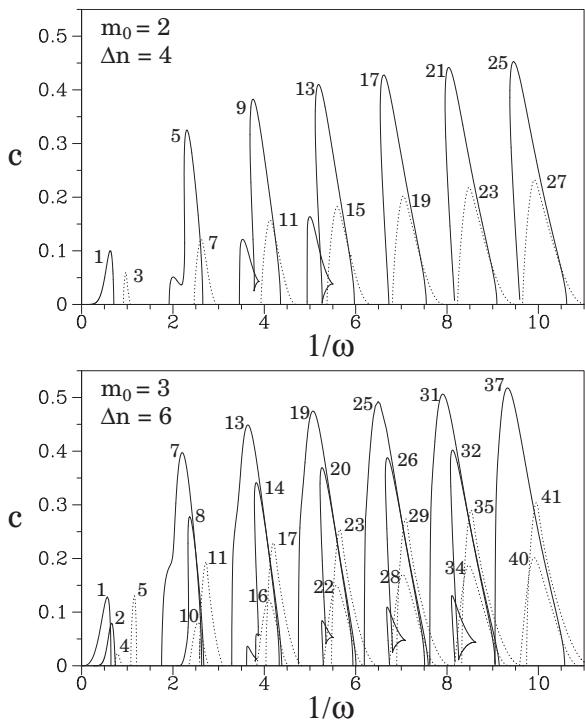


FIG. 17. (Top) The first 14 bifurcation lines generated by an esn bifurcation of period 2 for the $(c\omega)$ -Duffing oscillator. There exist two classes of period-2 bifurcations, the one with winding numbers given in Eq. (16) (solid line) and the second class with the “missing” winding numbers (dotted line). (Bottom) The first bifurcation lines generated by an esn bifurcation of period 3 for the $(c\omega)$ -Duffing oscillator. There exist four classes of period-3 bifurcations when looking at the maxima of the horns. They define a virtual line that grows monotonously in the parameter space. The numbers that characterize the lines are given by the torsion numbers of the bifurcations.

in Eq. (5)—one obtains

$$w = \frac{p}{q} : \frac{17}{3} \xrightarrow{+5} \frac{22}{4} \xrightarrow{+5} \frac{27}{5} \xrightarrow{+5} \frac{32}{6} \xrightarrow{+5} \frac{37}{7} \xrightarrow{+5} \frac{42}{8} \xrightarrow{+5} \dots$$

$$\begin{matrix} \xrightarrow{+5} \\ \xrightarrow{+1} \end{matrix}$$

(18)

which again leads to a formula for the sequence of winding numbers

$$p_1^l = l + 1, \quad q_1^l = 1, \quad l = 2, 4, 6, \dots,$$

$$w_k^l = \frac{p_k^l}{q_k^l} = \frac{(l + 1) + (l - 1)(k - 1)}{k}, \quad (19)$$

$$k = 1, 2, 3, \dots,$$

with the limit value

$$w_\infty^l = \lim_{k \rightarrow \infty} w_k^l = l - 1. \quad (20)$$

This sequence slightly differs from the one found in [Eq. (5)], but the two sequences can be converted into each other simply by changing signs. Note that for the “resonance $R_{0,1}$ ” only one sequence has been found and therefore the sequence Eq. (19) starts at $l = 2$ instead of $l = 0$.

It is now possible to calculate the k th main window appearing through an esn bifurcation for every even-numbered

resonance l of the Duffing oscillator via the formula

$$\begin{aligned} p_1^l &= l \pm 1, \quad q_1^l = 1, \quad l = 2, 4, 6, \dots, \\ w_k^l &= \frac{p_k^l}{q_k^l} = \frac{(l \pm 1) + (l \mp 1)(k-1)}{k}, \\ k &= 1, 2, 3, \dots, \end{aligned} \quad (21)$$

and the limit of either one sequence is given as

$$w_\infty^l = \lim_{k \rightarrow \infty} w_k^l = l \mp 1. \quad (22)$$

Empirically, it has been found that every resonance with even torsion number bears two distinct winding-number sequences. The only exception is the resonance $R_{0,1}$ where only one sequence has been found. The winding number of one of these sequences begins at $w_1^l = l + 1$ and converges to $w_\infty^l = l - 1$, and vice versa for the second winding-number sequence: $w_1^l = l - 1$ and $w_\infty^l = l + 1$.

For the $(c\omega)$ -Duffing oscillator we attempted to calculate all the bifurcation curves of period 3 that represent esn bifurcations. All these curves (Fig. 17, bottom diagram) are $\text{sn}(n,3)$ curves. The torsion number n is marked near the tip of each curve. The figure suggests to classify all of the period-3 curves shown into four distinct classes ($n_a = 1, 7, 13, 19, \dots$; $n_b = 2, 8, 14, 20, \dots$; $n_c = 4, 10, 16, 22, \dots$; $n_d = 5, 11, 17, 23, \dots$). Each of those four classes are arranged along an imaginary curve in the parameter space that connects the tip of the members of each class (compare with [11]) with torsion numbers that differ from their neighbors within each group by $\Delta n = 6$.

The two classes that are shown with a solid line style represent the elements of period- $m_0 = 3$ bifurcation curves (for $q = 3$ and $q = 6$) that obey the winding-number sequence of Eq. (5). At the bifurcation curves with odd torsion numbers, a periodic window arises by a sn bifurcation of a symmetric orbit. Two coexisting asymmetric orbits occur at the bifurcation points with even torsion numbers. In the same manner, the curves shown in the dotted line style are related. However, these two classes represent the periodic windows with the symmetry period numbers $q = 3$ and $q = 6$ that obey the sequence given by Eq. (19). No other bifurcation curves of period 3 that could be considered esn-bifurcation curves have been found during our investigations.

The periodic windows with symmetry period number $q = 4$ are found as windows with two coexisting period-2 orbits. All the bifurcation curves of period 2 with odd torsion number—windows with even torsion number could not be found—are shown in the top diagram of Fig. 17. These curves can again be divided into two classes: those that belong to the $q = 4$ window obeying Eq. (5) (solid lines) and those in the $q = 4$ window obeying Eq. (19) (dotted lines). In both cases it is $\Delta n = 4$.

Similarly, the number of different classes of period-5 esn bifurcations could be expected as $N = 2m - 2 = 8$. The “ -2 ” indicates the forbidden fractions $5/5$ and $10/5$ between two even numbers. Seven of these expected eight classes have been found and are shown in Fig. 18. Not every element of every class had been observed, though. The curves with the last digit being 3 represent the $q = 5$ windows of the sequence Eq. (5). The ones with the last digit being 4 represent the $q = 10$

windows of that same sequence. The ones with the last digit being 7 represent the $q = 5$ windows of the sequence Eq. (19). The corresponding curves for the $q = 10$ windows—torsion numbers ending in 6—could not be found, but a comparison with the $q = 5$ and $q = 10$ curves of sequence Eq. (5) suggests that these sn curves should be likely to be found for higher resonances (torsion numbers). Also, the last-digit-4 curves have not been found for the lower torsion numbers $n = 4$ and $n = 14$. For all sequences it is $\Delta n = 10$.

Each of the classes found for the $m_0 = 2$ and $m_0 = 3$ esn-bifurcation curves can be described with the help of the two winding-number sequences Eqs. (5) and (19). They are found to serve a particular role within the two winding-number sequences. For the $m_0 = 5$ curves, however, only four of the eight classes appear within these two sequences. This leads to the assumption that other winding-number sequences, similar in construction but likely more complex than the ones already found, may exist whereby the remaining four classes of bifurcation curves might be classified.

V. WINDOW SEQUENCES OF ASYMMETRIC OSCILLATORS

Winding-number sequences of the symmetric Duffing-type oscillator have been found. Together with the work by Scheffczyk *et al.* [11], we expect that our hitherto analysis could be generalized to a large class of different systems. Since it is known that many features of symmetric systems have their counterpart within asymmetric systems and vice versa, an open question is whether similar winding-number sequences can be found for asymmetric systems. With this regard, the bubble oscillator [8,9,29] has been adopted as an example for the class of asymmetric, strictly dissipative systems. A model for a spherical bubble in water with damping by sound radiation and viscosity of the liquid is chosen,

$$\left(1 - \frac{\dot{R}}{c}\right) R \ddot{R} + \frac{3}{2} \dot{R}^2 \left(1 - \frac{\dot{R}}{3c}\right) = \frac{P}{\rho} + \frac{1}{\rho c} \frac{d(RP)}{dt}, \quad (23)$$

where

$$\begin{aligned} P(R, \dot{R}, t) &= \left(p_{\text{stat}} - p_v + \frac{2\sigma}{R_n}\right) \left(\frac{R_n}{R}\right)^{3\kappa} - p_{\text{stat}} \\ &+ p_v - \frac{2\sigma}{R} - \frac{4\mu}{R} \dot{R} - p(t), \end{aligned} \quad (24)$$

$$p(t) = p_a \sin(2\pi \nu_a t). \quad (25)$$

The variables and parameters are the bubble radius R as a function of time t , its time derivative \dot{R} , its second time derivative \ddot{R} , the bubble radius at rest R_n , the frequency of the driving sound field ν_a , the amplitude of the driving sound field p_a , the static (ambient) pressure $p_{\text{stat}} = 100$ kPa, the vapor pressure of the liquid (water) $p_v = 2.33$ kPa, the surface tension $\sigma = 0.0725$ N/m, the ratio of the specific heats of the gas inside the bubble $\kappa = 1.67$ (noble gas), the viscosity of the liquid $\mu = 0.001$ Pa s, the sound velocity of the liquid $c = 1500$ m/s, and the density of the liquid $\rho = 998$ kg/m³.

A typical bifurcation diagram for the system is shown in Fig. 19 with the frequency ν_a of the sound field as control parameter. The remaining not yet specified parameters were

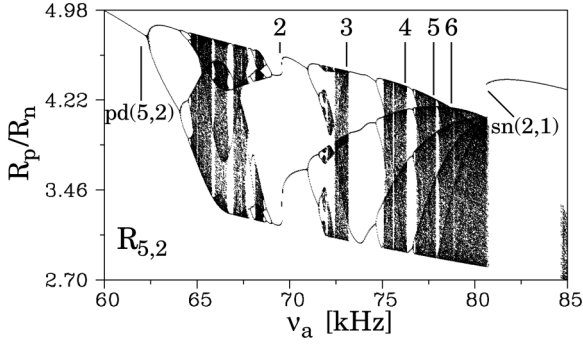


FIG. 19. Bifurcation diagram for the bubble oscillator in a Poincaré section plane. Depicted is the diagram for $R_n = 10 \mu\text{m}$, $p_a = 160 \text{ kPa}$. This is an asymmetric system showing a sequence of periodic windows in the resonance $R_{5,2}$.

chosen to be $R_n = 10 \mu\text{m}$ and $p_a = 160 \text{ kPa}$. The resonance $R_{5,2}$ is shown in this diagram and periodic windows with increasing period can be detected up to a small window of period 6. For asymmetric systems the symmetry period number q is always $q = m_0$, since for these systems only asymmetric orbits can occur. The bifurcation diagram looks similar to the one presented earlier for the Duffing oscillator (Fig. 3) and therefore a similar winding-number sequence of sn bifurcations can be expected.

Writing down the winding numbers of the sn-bifurcation points in the same way as has been done for the Duffing oscillator, the following sequence for the resonance $R_{5,2}$ is obtained:

$$w = \frac{n}{m} : \frac{3}{1} \xrightarrow{+2} \frac{5}{2} \xrightarrow{+2} \frac{7}{3} \xrightarrow{+2} \frac{9}{4} \xrightarrow{+2} \frac{11}{5} \xrightarrow{+2} \frac{13}{6} \xrightarrow{+2} \dots$$

$$\begin{array}{cccccc} \curvearrowright & \curvearrowright & \curvearrowright & \curvearrowright & \curvearrowright & \curvearrowright \\ \curvearrowleft & \curvearrowleft & \curvearrowleft & \curvearrowleft & \curvearrowleft & \curvearrowleft \end{array}$$

(26)

This sequence can be written as a formula similar to Eqs. (5) and (19), but the interpretation of the different terms differs slightly due to the asymmetry:

$$n_1^l = l, \quad m_1^l = 1, \quad l = 1, 2, 3, 4, \dots,$$

$$w_k^l = \frac{n_k^l}{m_k^l} = \frac{l + (l-1)(k-1)}{k}, \quad k = 1, 2, 3, 4, \dots$$

(27)

For asymmetric systems all resonances with period $m_0 = 1$ are isn bifurcations. Within these resonances there are no pd bifurcations and therefore no window sequences can be found. Consequently, the index l does not indicate all of the occurring resonances but only the ones within which period-doubling cascades can be found. This is the case for all resonances $R_{n,2}$ and the index l can be obtained as $l = \lceil n/2 \rceil$, i.e., the next integer larger than $n/2$ (e.g., $R_{5,2} \rightarrow \lceil 2.5 \rceil = 3$).

The sequence starts for $k = 1$ with the winding number $w_1^l = n_1^l/m_1^l = 3/1$. This is the winding number of the sn bifurcation of the following resonance with period 1 ($R_{3,1}$) to be found towards the lower frequencies v_a in this example.

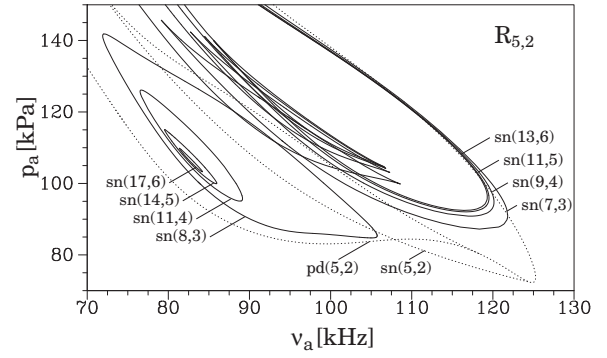


FIG. 20. The first four bifurcation curves of the two different winding-number sequences of the resonance $R_{5,2}$ of the bubble oscillator. The dotted lines have winding number $w = 5/2$. The pd curve embraces both sequences; the sn curve dissects them.

The winding number for $k = 2$ corresponds to the first pd bifurcation ($w_2^l = 5/2$) of the resonance. In comparison, the winding number for symmetric systems at $k = 2$ corresponds to a sb bifurcation. As known from [33] the sb bifurcation of a symmetric system is just the first pd bifurcation of a corresponding asymmetric system with half the period. Therefore, the first two winding numbers of the sequences for symmetric and asymmetric systems correspond and represent exemptions to the sequences in the same sense as explained above, since they do not represent the occurrence of periodic windows.

The winding numbers for $k = 3, 4, 5, \dots$ are found again at the bifurcation points, where periodic orbits arise out of the chaotic region.

The limiting value of the sequence Eq. (27) is given as

$$w_\infty^l = \lim_{k \rightarrow \infty} w_k^l = l - 1. \quad (28)$$

The bifurcation curves belonging to the periodic windows in Fig. 19 and formed by sn bifurcations are shown in Fig. 20.

The curve for the pd bifurcation, pd(5,2), is shown as a dotted line that acts, in some sense, as an envelope of the esn curves of the winding-number sequence. A second dotted line shows the sn(5,2) curve which separates the pd(5,2) resonance into two parts. As has been found for the symmetric systems, the asymmetric systems also show a second set of sn-bifurcation curves [left side of the sn(5,2) resonance in Fig. 20]. The respective winding numbers can be ordered in the following way, representing a different winding-number sequence:

$$w = \frac{n}{m} : \frac{2}{1} \xrightarrow{+3} \frac{5}{2} \xrightarrow{+3} \frac{8}{3} \xrightarrow{+3} \frac{11}{4} \xrightarrow{+3} \frac{14}{5} \xrightarrow{+3} \frac{17}{6} \xrightarrow{+3} \dots$$

$$\begin{array}{cccccc} \curvearrowright & \curvearrowright & \curvearrowright & \curvearrowright & \curvearrowright & \curvearrowright \\ \curvearrowleft & \curvearrowleft & \curvearrowleft & \curvearrowleft & \curvearrowleft & \curvearrowleft \end{array}$$

(29)

This sequence can be written as

$$n_1^l = l - 1, \quad m_1^l = 1, \quad l = 1, 2, 3, 4, \dots,$$

$$w_k^l = \frac{n_k^l}{m_k^l} = \frac{(l-1) + l(k-1)}{k}, \quad k = 1, 2, 3, 4, \dots, \quad (30)$$

with the limit

$$w_\infty^l = \lim_{k \rightarrow \infty} w_k^l = l. \quad (31)$$

Comparing Eqs. (27) and (30), their difference is given by just changing the term $(l - 1)$ to l and vice versa.

VI. UNIFYING ASYMMETRIC AND SYMMETRIC SYSTEMS

Our numerical investigations suggest that one-dimensional, strictly dissipative oscillators show the existence of two regular winding-number sequences within every resonance that exhibits chaos. Chaos can be found at resonances $R_{2n,1}$ of period 1 and even torsion number in the case of symmetric systems and at resonances $R_{2n-1,2}$ of period 2 with odd torsion number in the case of asymmetric systems.

The common behavior of both types of systems in regard to their winding-number sequences can be merged into a single formula that combines Eqs. (5), (19), (27), and (30) as

$$w_k^l = \frac{(l \pm 1) + (l \mp 1)(k - 1)}{k}, \quad (32)$$

with $k = 1, 2, 3, \dots$ and

$$\left. \begin{aligned} l = 2, 4, 6, \dots & \quad \text{if symmetric,} \\ l = 1, 2, 3, \dots & \quad \text{if asymmetric.} \\ (l + 1) \rightarrow l & \end{aligned} \right\}$$

The limiting value of Eq. (32) is given by

$$w_\infty^l = (l \mp 1) \quad \text{with} \quad (l + 1) \rightarrow l \quad \text{if asymmetric.} \quad (33)$$

The meaning of this equation for both types of nonlinear systems is shown in a schematic manner in Fig. 21.

For symmetric systems (bottom diagram of Fig. 21) the winding-number sequences can be found between the resonances $R_{2n-1,1}$ and $R_{2n+1,1}$. The curve of the $sb(2n, 1)$ bifurcation is divided into two parts by the $sn(2n, 1)$ bifurcation. On both sides of the $sn(2n, 1)$ bifurcation one winding-number sequence can be found. The winding numbers of these esn bifurcations are governed by Eq. (27). On the side of the sb curve facing the resonance $R_{1,1}$ (e.g., the resonance with lower torsion number $R_{2n-1,1}$), the first element w_1^l of the sequence is equal to the torsion number of the higher resonance $R_{2n+1,1}$ of period 1 [$w_1^l = (l + 1)$]. The limit of that sequence equals the odd torsion number of the lower resonance $R_{2n-1,1}$ [$w_\infty^l = (l - 1)$]. The transition from $(l + 1)$ to $(l - 1)$ is marked at the bottom of the diagram. A cross section, for which this transition of the winding numbers at esn bifurcations can be observed, is suggested by a big arrow. The sequence on the right side of resonance $R_{2n,1}$ shows the reversed behavior and the terms $(l + 1)$ and $(l - 1)$ have to be interchanged.

For the asymmetric systems an analogous behavior can be found (see the top diagram of Fig. 21). The window sequences can only be found in resonances $R_{2n-1,2}$. As a result, the index l is not limited to even numbers. Therefore, the window sequence on the left hand side of the asymmetric diagram shows the transition $w_1^l = l \Rightarrow w_\infty^l = (l - 1)$. Again, the sequence to the right of the bifurcation $sn(2n - 1, 2)$ has interchanged (l) with $(l - 1)$.

For all systems and resonances that we have investigated, one of the two window sequences seem to be dominant and

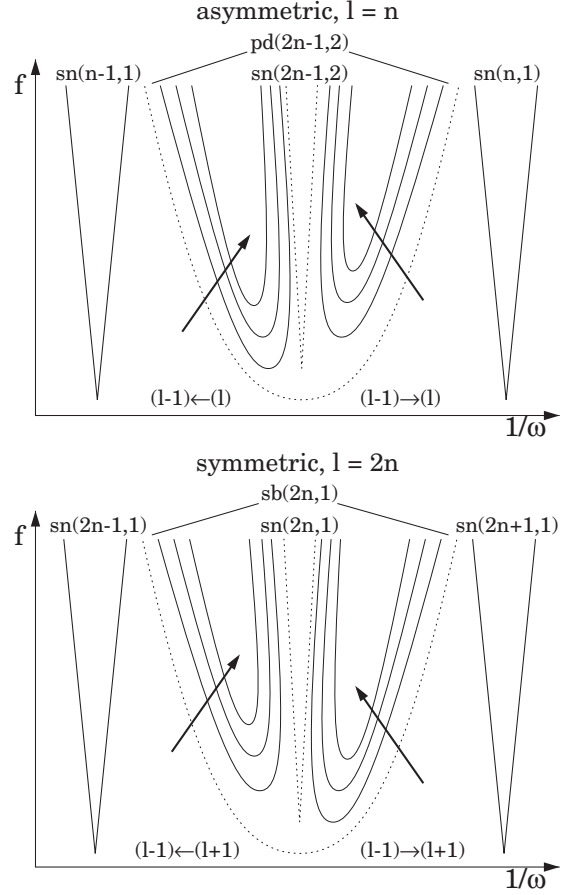


FIG. 21. Topological sketch of the two winding-number sequences as they occur in asymmetric and symmetric systems. The arrows indicate the paths in the parameter space along which periodic windows with increasing period can be found.

concealing the other sequence. Those concealed sequences were only found by calculating the bifurcation curves after their existence had been suspected from the respective formulas rather than being suggested by looking at bifurcation diagrams. For the symmetric systems this was true for the sequences with the transition from $(l - 1)$ to $(l + 1)$ (bottom diagram in Fig. 21) and again the other way round for the asymmetric systems with the transition (l) to $(l - 1)$ (top diagram of Fig. 21).

It has not further been investigated, whether this is a common feature for these types of systems or if it would also be possible to investigate the minor sequences by means of bifurcation diagrams.

Looking at the individual elements of Eq. (21) it should be noted that for both sequences the value of the element w_2^l is identical. In some sense, this element can be regarded as the crossing point of both coexisting sequences within one resonance. This has been indicated with the help of Fig. 22 describing the sequences of an asymmetric system. In both the top and the bottom diagrams the elements of the two sequences are marked with the dark and light gray circles, respectively. In the top part of Fig. 22 the sequences are embedded within a Farey tree [31,34,35]. The periodic windows for a self-excited oscillator are ordered by means of the Farey tree, and as

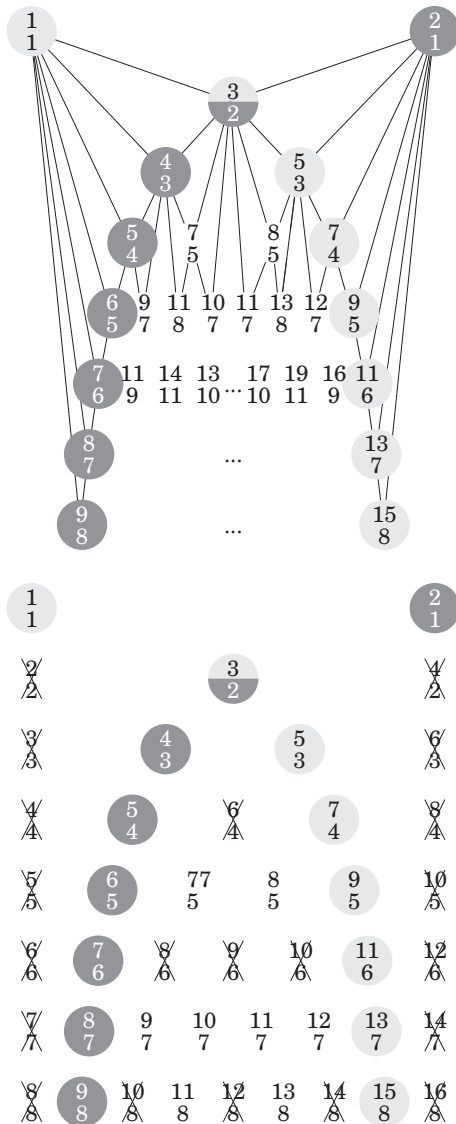


FIG. 22. Winding-number sequence for an asymmetric system for $l = 2$ in the graph of the Farey tree (top) and in the graph of all fractions with the period number increasing from row to row by one (bottom).

can be seen here, this is also the case (at least for the main windows) for strictly dissipative systems. The sequences of winding numbers build the outside borders of the Farey tree. This follows from the principle of the construction of the Farey tree, because, as the periodic windows increase, the period increases by one, just by definition of the outside elements of the Farey tree. However, trying to fit subsequences or pd sequences into this scheme of fractions was not successful. Obviously, the Farey tree construction must be extended for the inclusion of all the winding-number sequences found so far.

The bottom part of Fig. 22 shows every possible fraction with positive sign between $(l - 1) = 1$ and $(l) = 2$. This is in analogy to the sequences shown in Eqs. (15)–(17). Every row in this diagram lists the fractions within the interval $[1, 2]$ according to the denominator which increases by one for every row. All expanded fractions are crossed out to indicate that

those winding numbers have never been found numerically during our investigations when calculating bifurcation curves. Naturally, the remaining fractions can also be found within the Farey tree but ordered differently. The members of the two winding-number sequences can then be found as the outside elements of the remaining fractions. In this diagram, the transition from $w_1^l = 1$ towards $w_\infty^l = 2$ (and vice versa) is obvious and it can be expected that the remaining fractions within this diagram will play an important role for further sub- and subsubsequences yet to be explored.

In addition, this diagram underlines the existence of different classes of period- m_0 bifurcation curves mentioned above. There are one class of period 2, two classes of period 3, four of period 5, etc., as has been demonstrated in Figs. 17 and 18. Note that for symmetric systems the number of classes for every period m_0 has to be doubled compared to the asymmetric systems, because of the transition $(l - 1) \rightarrow (l + 1)$ instead of $(l - 1) \rightarrow (l)$.

VII. DISCUSSION

Periodically driven nonlinear oscillators show a multitude of resonances (large excursions of a dependent variable, e.g., an elongation and compression of a spring), when the driving frequency is altered. Every resonance can be assigned a rational number n/m that denotes its order [8]: $1/1$ is the main resonance (the only one in a linear oscillator), $2/1, 3/1, 4/1, \dots$, are the harmonic resonances (appearing at driving frequencies below the main resonance), $1/2, 1/3, 1/4, \dots$, are the subharmonic resonances (appearing at frequencies above the main resonance) and the remaining rational numbers are subsumed under the name of ultrasubharmonic resonances.

The complete diagram of the resonance system of an asymmetric oscillator, called the superstructure, is given in Fig. 23. In this diagram, the numbers in the circles and ovals n/m denote the order of the respective resonance $R_{n,m}$. The top row shows the first four of the harmonic resonances $R_{n,1}, n \in \mathbb{N}_0$, which are all of period 1: $R_{0,1}, R_{1,1}, R_{2,1}, R_{3,1}$. For insertion of the resonance $R_{0,1}$, see Sec. IV. The second row shows the resonances of period 2, the third row those of period 3, etc., whereby the Farey ordering is indicated by the network of solid lines. The vertical dashed lines are the loci of all expanded fractions $nr/mr, r \in \mathbb{N} \setminus 1$, that can be derived from the fraction n/m , wherefrom a dashed line originates. Because none of the resonances corresponding to expanded fractions have been found (see Fig. 22, bottom), they cannot serve as connecting resonances to cross a dashed line. The shortest way to reach the other side of a dashed line is via the resonance at the top of the respective dashed line.

The following resonances have been found for the bubble oscillator: the harmonic resonances of order $1/1, 2/1, 3/1$ and additionally (beyond the diagram given in Fig. 23) up to order $\sim 20/1$ [36]; the subharmonic resonances $1/2$ and $1/3$ [8]; the ultrasubharmonic resonances of order $3/2, 5/2$ and additionally (beyond the diagram given in Fig. 23) $7/2, 9/2, 11/2, 13/2$, and $15/2$ [37], as well as $2/3, 4/3, 5/3, 7/3$, and $2/5$ (see [8,36,38]). These resonances obey the Farey ordering, because the ultrasubharmonic resonances $3/2, 5/2, 7/2, 9/2, \dots$ are located between the harmonic resonances $1/1, 2/1, 3/1, 4/1, 5/1, \dots$ in the ordering $1/1, 3/2, 2/1, 5/2, 3/1,$

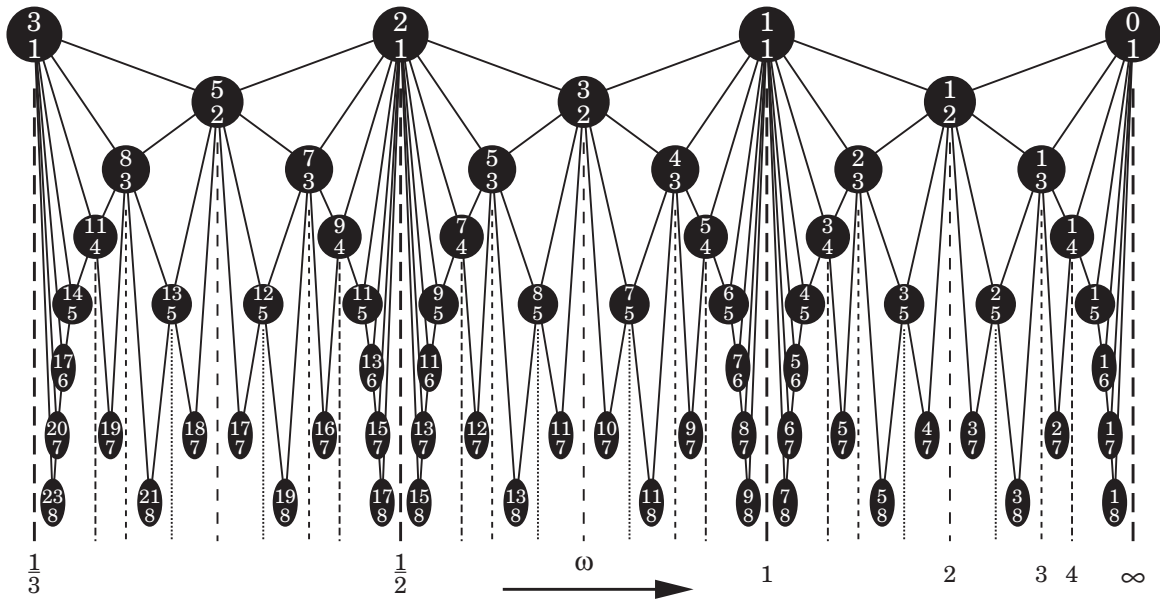


FIG. 23. Superstructure of an asymmetric oscillator. The Farey tree system extends further to the left, with the next harmonic resonances $4/1, 5/1, \dots$, the ultrasubharmonic resonances $7/2, 9/2, \dots$, and the higher periods. The diagram also extends further down to period numbers $m = 9, 10, \dots$, with torsion numbers n selected according to the Farey tree construction.

$7/2, 4/1, 9/2, 5/1, \dots$, as in the diagram of Fig. 23. The ultrasubharmonic resonances $2/3, 4/3, 5/3$, and $7/3$ appear at the second level and are found between the resonances $1/2$ and $1/1, 1/1$ and $3/2, 3/2$ and $2/1$, and $2/1$ and $5/2$, respectively [38]. The resonance $2/5$ appears and has been found between the resonances $1/3$ and $1/2$ [8]. A similar set of resonances has been found in the pump modulated laser oscillator [10] obeying the superstructure as given in Fig. 23.

This ordering most completely appears at low damping and can be understood by the nonlinearity term in the differential equation that mixes the frequency components of the resulting oscillation, thereby transferring energy from the main resonance along a cascade of further resonances down to the resonances of higher order (larger n and m). Subharmonic [39] and ultrasubharmonic resonances have driving-amplitude onset thresholds that depend on the damping of the oscillator. Higher order resonances have higher thresholds and thus may be suppressed. In that case, the superstructure terminates in a specific way before the respective Farey sequences are complete. This gives each resonance horn its specific structure.

The ultrasubharmonic resonances may be captured by a neighboring resonance of lower order inside its hysteresis region at higher driving (see [9], Fig. 12). Due to the Farey ordering of the resonances, the higher Farey resonances in between lower ones are then generically included in the capturing process giving rise to the inner structure of the respective resonance (depending on the damping that may suppress higher order resonances). The interior of the resonances thus shows an involved structure, each resonance with its specific properties. This structure has been investigated here in more detail for the resonance $R_{6,1}$ of the $(-, +)$ -Duffing oscillator (see also [12]), the resonance $R_{5,2}$ of a bubble oscillator [27], and the first few harmonic resonances of the $(c\omega)$ -Duffing oscillator by concentrating on the periodic windows and their winding numbers.

For the case of the resonance $R_{6,1}$ Gilmore and McCallum [40] have constructed a geometric abstract of a chaotic attractor, called a template. The mathematical operation they use, however, is not equivalent to increasing the damping of the oscillator. Increased damping also operates on the window structure in the sense of suppressing resonances and the associated window sequences. With the help of the template they could develop a symbolic dynamics for the ordering of the most prominent periodic windows. Opposite to their assumption, however, it is shown here that it is not always the largest windows in width that have to be accumulated into a sequence (see Fig. 5, bottom diagram).

The first approach of ordering by a Farey tree can be found in [29], Fig. 25. It has a quite different ordering from that in [40] in that it has the same period numbers on the same level. This ordering has not been discussed in [40]. Instead, two small asymmetric parts of the full Farey tree are given. Figure 23, moreover, has a quantitative parameter axis (ω) for showing the clustering of winding numbers.

As an extension to the investigation of harmonic resonances the window structure inside an ultrasubharmonic resonance ($5/2$) of the superstructure has been investigated for its winding-number sequences. It again shows period adding (Fig. 22) and an accompanying window structure. This structure additionally is buried in resonances of lower order (here between $R_{3,1}$ and $R_{2,1}$) in a nested way. The nesting of resonances gives rise to a proliferation of periodic windows. Once the period-adding sequences in each resonance are complete, infinitely many windows multiplied by infinitely many windows are present in each resonance. The ordering of these windows may be impossible to formulate in terms of simple laws. Perhaps special routes through the parameter space may facilitate an ordering.

It is the Farey ordering from the energy transfer cascade that determines the features of the superstructure. The universality

of the bifurcation structure for different nonlinear oscillators then is of physically determined origin (frequency mixing). Special details are nevertheless present because of the shape (hard or soft spring behavior) and strength of the nonlinearity and, of course, symmetry properties.

Another approach to finding periodic windows for their classification is via determination of the Lyapunov spectrum of the dynamical system in question. Period-adding sequences have been found by Bonatto *et al.* [5] for the (0,+)-Duffing oscillator with a period-adding number of 3 given explicitly. No torsion or winding numbers have been calculated, however. This has been done by Medeiros *et al.* [41] and the authors suggest torsion adding in addition to period adding to group windows into sequences, as has been done here as well; see Eqs. (16)–(18). Medeiros *et al.* suggest a general formula where both sequences are combined and test it for the Morse oscillator, an asymmetrical oscillator; see also [25] and the topological equivalence of nonlinear oscillators in [11]. They rely on the skeleton construction for the circle map of degree 1 [42,43] (see also Ref. [44] for a two-dimensional map) and find skeleton sequences for the Morse oscillator in the two-parameter space of driving frequency and damping for one constant driving amplitude. The sequences have been constructed by period adding and torsion adding with a constant value, each leaving many skeletons in between. Their ordering (regular or chaotic) is still an open question as it is for the many subsubwindows encountered here in the one-dimensional cuts along the frequency axis for the case of the (−,+)-Duffing oscillator.

Parameter-plane plots of periodic windows may help to construct ordered sequences when combined with bifurcation diagrams along selected lines through a parameter plane. This concept has been followed by Rech [45] for a much more complicated problem, the periodically forced KdV-Burgers equation, a nonlinear partial differential equation of third order. It is transformed to a nonlinear autonomous system of three first order ordinary differential equations by looking for traveling wave solutions that eliminate the partial time derivative. Interestingly, the result is a special type of asymmetric double-well Duffing oscillator:

$$\ddot{x} + \mu\dot{x} - \alpha x + \beta x^2 + \delta x^3 = g \cos(\omega t). \quad (34)$$

This type of Duffing oscillator seems to belong to the class of oscillators investigated here, because a complex network of windows of similar structure is found that reveals involved sequences similar to the ones found in Fig. 5. The sequences can be arranged in a very complex ordering of periods [45]. However, at least some of them can also be considered as being composed of interlaced series with just period-adding properties (compare Figs. 17 and 18). As Lyapunov calculations

do not supply connectivity information, the calculation of fixed-point curves together with torsion and winding numbers for grouping of windows into sequences, as done here, would solve questions of ordering.

VIII. CONCLUSIONS

Periodic windows inside resonances of driven nonlinear oscillators have been investigated. Each resonance is characterized by its own hierarchy of winding-number sequences for its periodic windows. Some empirical laws for the first two hierarchy levels have been found. At the first level, a series of windows, called main windows, with period adding can be constructed, whose winding numbers obey Eq. (5) or (19) for symmetric systems and Eq. (27) or (30) for asymmetric systems. A sketch of the topology of the phase diagram connected to these series of bifurcations is given in Fig. 21. The period adding implies that there are as many main windows as there are natural numbers. This holds for every resonance.

At the second level, a series of windows, called subwindows, can be constructed which also shows period adding. The subwindows reside within the chaotic band that exists between each two adjacent main windows and each chaotic band contains a finite number of them. This number increases by one for consecutive chaotic bands. Thus, there are as many subwindows as the sum of the natural numbers. A formula for the winding numbers of the subwindows is given in Eq. (12).

A deeper investigation of the window hierarchy is limited by the proliferation of very small windows that are hard to identify precisely. Surely, there will be more than the sum of the natural numbers on the proposed third level of subsubwindows.

Finally, our study shows that the periodic solutions of different types of oscillators that occur as windows in bifurcation diagrams can be subject to an ordering scheme whose first elements could be given here. These elements can be considered as the first steps for a description of the bifurcation set of a certain class of driven nonlinear oscillators.

ACKNOWLEDGMENTS

We would like to thank the members of the Nonlinear Dynamics group of the Institut für Angewandte Physik, Technische Hochschule Darmstadt, for their constant support. Special gratitude goes to C. Scheffczyk, M. Wiesenfeldt, T. Kurz, R. Mettin, and J. Holzfuss. Without their helpful discussions, support, and effort this work would not have been possible. In addition, we would like to thank C. Scheffczyk for entrusting to us his software package YACOP for the calculations of the fixed-point curves and phase diagrams.

-
- [1] S.-i. Sato, M. Sano, and Y. Sawada, Universal scaling property in bifurcation structure of Duffing's and of generalized Duffing's equations, *Phys. Rev. A* **28**, 1654 (1983).
 [2] H. Kawakami, Bifurcation of periodic responses in forced dynamic nonlinear circuits: Computation of bifurcation values

of the system parameters, *IEEE Trans. Circuits Syst.* **31**, 248 (1984).

- [3] U. Parlitz and W. Lauterborn, Superstructure in the bifurcation set of the Duffing equation $\ddot{x} + d\dot{x} + x + x^3 = f \cos(\omega t)$, *Phys. Lett. A* **107**, 351 (1985).

- [4] U. Parlitz, Common dynamical features of periodical driven strictly dissipative oscillators, *Int. J. Bifurcation Chaos Appl. Sci. Eng.* **3**, 703 (1993).
- [5] C. Bonatto, J. A. C. Gallas, and Y. Ueda, Chaotic phase similarities and recurrences in a damped-driven Duffing oscillator, *Phys. Rev. E* **77**, 026217 (2008).
- [6] I. S. Stefanescu, The onset of bifurcations in the forced Duffing equation with damping, *Int. J. Bifurcation Chaos Appl. Sci. Eng.* **23**, 1330006 (2013).
- [7] R. Gilmore and M. Lefranc, *The Topology of Chaos* (Wiley, New York, 2002).
- [8] W. Lauterborn, Numerical investigation of nonlinear oscillations of gas bubbles in liquids, *J. Acoust. Soc. Am.* **59**, 283 (1976).
- [9] W. Lauterborn and T. Kurz, Physics of bubble oscillations, *Rep. Prog. Phys.* **73**, 106501 (2010).
- [10] W. Lauterborn and R. Steinhoff, Bifurcation structure of a laser with pump modulation, *J. Opt. Soc. Am. B* **5**, 1097 (1988).
- [11] C. Scheffczyk, U. Parlitz, T. Kurz, W. Knop, and W. Lauterborn, Comparison of bifurcation structures of driven dissipative nonlinear oscillators, *Phys. Rev. A* **43**, 6495 (1991).
- [12] V. Englisch and W. Lauterborn, Regular window structure of a double-well Duffing oscillator, *Phys. Rev. A* **44**, 916 (1991).
- [13] G. Eilenberger and K. Schmidt, Poincaré maps of Duffing type oscillators and their reduction to circle maps: I. Analytic results, *J. Phys. A: Math. Gen.* **25**, 6335 (1992).
- [14] K. Schmidt and G. Eilenberger, Poincaré maps of Duffing type oscillators and their reduction to circle maps: II. Methods and numerical results, *J. Phys. A: Math. Gen.* **31**, 3903 (1998).
- [15] P. Beiersdorfer, J. M. Wersinger, and Y. Treve, Topology of the invariant manifolds of period-doubling attractors for some forced nonlinear oscillators, *Phys. Lett. A* **96**, 269 (1983).
- [16] P. Beiersdorfer, Universality of topology of period doubling dynamical systems, *Phys. Lett. A* **100**, 379 (1984).
- [17] U. Parlitz and W. Lauterborn, Resonances and torsion numbers of driven dissipative nonlinear oscillators, *Z. Naturforsch. A* **41**, 605 (1986).
- [18] J. M. Perez, Mechanism for global features of chaos in a driven nonlinear oscillator, *Phys. Rev. A* **32**, 2513 (1985).
- [19] S. D. Brorson, D. Dewey, and P. S. Linsay, Self-replicating attractor of a driven semiconductor oscillator, *Phys. Rev. A* **28**, 1201(R) (1983).
- [20] G. Vazquez, C. Camara, S. Putterman, and K. Weninger, Sonoluminescence: nature's smallest blackbody, *Opt. Lett.* **26**, 575 (2001).
- [21] D. J. Flannigan and K. S. Suslick, Inertially confined plasma in an imploding bubble, *Nat. Phys.* **6**, 598 (2010).
- [22] P. Koch, T. Kurz, U. Parlitz, and W. Lauterborn, Bubble dynamics in a standing sound field: The bubble habitat, *J. Acoust. Soc. Am.* **130**, 3370 (2011).
- [23] D. Schanz, B. Metten, T. Kurz, and W. Lauterborn, Molecular dynamics simulation of cavitation bubble collapse and sonoluminescence, *New J. Phys.* **14**, 113019 (2012).
- [24] D. F. Gaitan, L. A. Crum, C. C. Church, and R. A. Roy, Sonoluminescence and bubble dynamics for a single, stable cavitation bubble, *J. Acoust. Soc. Am.* **91**, 3166 (1992).
- [25] W. Knop and W. Lauterborn, Bifurcation structure of the classical Morse oscillator, *J. Chem. Phys.* **93**, 3950 (1990).
- [26] V. Englisch and W. Lauterborn, The winding-number limit of period-doubling cascades derived as Farey-fraction, *Int. J. Bifurcation Chaos Appl. Sci. Eng.* **4**, 999 (1994).
- [27] V. Englisch, Über periodische Fenster nichtlinearer Oszillatoren (On periodic windows of nonlinear oscillators), Ph.D. thesis, Technical University of Darmstadt, Germany, 1993.
- [28] C. Scheffczyk (private communication).
- [29] U. Parlitz, V. Englisch, C. Scheffczyk, and W. Lauterborn, Bifurcation structure of bubble oscillators, *J. Acoust. Soc. Am.* **88**, 1061 (1990).
- [30] T. Kurz and W. Lauterborn, Bifurcation structure of the Toda oscillator, *Phys. Rev. A* **37**, 1029 (1988).
- [31] R. Mettin, U. Parlitz, and W. Lauterborn, Bifurcation structure of the driven Van der Pol oscillator, *Int. J. Bifurcation Chaos Appl. Sci. Eng.* **3**, 1529 (1993).
- [32] T. Klinker, W. Meyer-Ilse, and W. Lauterborn, Period doubling and chaotic behavior in a driven Toda oscillator, *Phys. Lett. A* **101**, 371 (1984).
- [33] J. W. Swift and K. Wiesenfeld, Suppression of Period Doubling in Symmetric Systems, *Phys. Rev. Lett.* **52**, 705 (1984).
- [34] W. Lauterborn and I. Eick, Numerical investigation of a periodically driven laser with an intracavity saturable absorber, *J. Opt. Soc. Am. B* **5**, 1089 (1988).
- [35] U. Parlitz and W. Lauterborn, Period-doubling cascades and devil's staircases of the driven van der Pol oscillator, *Phys. Rev. A* **36**, 1428 (1987).
- [36] W. Lauterborn and R. Mettin, Nonlinear bubble dynamics - Response curves and more, in *Sonochemistry and Sonoluminescence*, edited by L. A. Crum *et al.* (Kluwer, Dordrecht, 1999), pp. 63–72.
- [37] W. Lauterborn and E. Cramer, Subharmonic Route to Chaos Observed in Acoustics, *Phys. Rev. Lett.* **47**, 1445 (1981).
- [38] E. Cramer and W. Lauterborn, Zur Dynamik und Schallabstrahlung kugelförmiger Kavitationsblasen in einem Schallfeld (On the dynamics and sound emission of spherical cavitation bubbles in a sound field), *Acustica* **49**, 226 (1981).
- [39] A. Prosperetti, A general derivation of the subharmonic threshold for non-linear bubble oscillations, *J. Acoust. Soc. Am.* **133**, 3719 (2013).
- [40] R. Gilmore and J. W. L. McCallum, Structure in the bifurcation diagram of the Duffing oscillator, *Phys. Rev. E* **51**, 935 (1995).
- [41] E. S. Medeiros, T. R. O. Medrano, I. L. Caldas, and S. L. T. de Souza, Torsion-adding and asymptotic winding number for periodic window sequences, *Phys. Lett. A* **377**, 628 (2013).
- [42] J. Bélair and L. Glass, Universality and self-similarity in the bifurcation of circle maps, *Physica D* **16**, 143 (1985).
- [43] L. Glass and R. Perez, Fine Structure of Phase Locking, *Phys. Rev. Lett.* **48**, 1772 (1982).
- [44] J. A. C. Gallas, Structure of the Parameter Space of the Hénon Map, *Phys. Rev. Lett.* **70**, 2714 (1993).
- [45] P. C. Rech, Nonlinear dynamics investigation in parameter planes of a periodically forced compound KdV-Burgers equation, *Eur. Phys. J. B* **86**, 356 (2013).